Materials Advances

ROYAL SOCIETY OF CHEMISTRY

REVIEW

View Article Online
View Journal | View Issue

Cite this: *Mater. Adv.*, 2024, 5, 2689

Anti-corrosion properties of bio-inspired surfaces: a systematic review of recent research developments

Qingyun Ma,[a] Qing Yang,*[b] Jialiang Zhang,[a] Fangzheng Ren,[a] Chongxiao Xia[a] and Feng Chen *[a]

Strengthening measures for protecting metals against corrosion hold significant importance for environmental preservation, economic development, and the enhancement of people's well-being. It is crucial to research and implement effective protection technologies. Bio-inspired surfaces have emerged as a compelling avenue in corrosion protection research, owing to their unique design and functionality. This paper delves into the key findings and innovations in bio-inspired surfaces for anticorrosion through a systematic review organized into three distinct parts, each focusing on a specific category of bio-inspired coatings. In the first part, the paper examines self-healing coatings inspired by the regenerative properties of skin. Emphasis is placed on how the design and composition of these coatings draw inspiration from the remarkable self-repair ability of the skin. The second part delves into superhydrophobic coatings inspired by the lotus plant. The paper systematically presents the design curation, structural features, and research progress of superhydrophobic surfaces, with a focus on their role in self-cleaning, anti-pollution, and anti-corrosion. The third part explores slippery liquid-infused porous surfaces (SLIPSs) inspired by lubricating plants and animals, such as Nepenthes. This section provides a systematic overview of research advances in SLIPSs and their potential applications in corrosion protection. Through this systematic review, this paper offers a comprehensive perspective on various strategies employed in bio-inspired surfaces for corrosion protection. By summarizing and reviewing the latest developments in self-healing, superhydrophobic, and SLIPS surfaces, this paper provides valuable insights into current advancements in the field.

Received 29th November 2023,
Accepted 6th February 2024

DOI: 10.1039/d3ma01058a

rsc.li/materials-advances

[a] *State Key Laboratory for Manufacturing System Engineering and Shaanxi Key Laboratory of Photonics Technology for Information, School of Electronic Science and Engineering, Xi'an Jiaotong University, Xi'an 710049, P. R. China. E-mail: chenfeng@mail.xjtu.edu.cn*
[b] *School of Instrument Science and technology, Xi'an Jiaotong University, Xi'an 710049, P. R. China. E-mail: yangqing@mail.xjtu.edu.cn*

Qingyun Ma

Dr Qingyun Ma is currently a PhD student in Prof. Feng Chen's group at Xi'an Jiaotong University. His research interests include bio-inspired design for corrosion, fouling and drag reduction.

Qing Yang

Prof. Qing Yang received her BS degree in Photoelectron Science and Technology in 1992 from Sichuan University. In 2009, she received her PhD from Xi'an Institute of Optics and Fine Mechanics, Chinese Academy of Science. She is currently an associate professor at Xi'an Jiaotong University. Her current research interests are femtosecond laser micro- and nanofabrication, laser biomimetic micro- and nanofabrication, ultrafast photonics and micro- and nanophotonics.

Introduction

Metals and alloys are extensively utilized in various industries such as engineering, transportation, construction, marine, and aerospace. However, these metallic materials are prone to corrosion when exposed to different environmental factors.[1–5] Corrosion is a pervasive issue that leads to significant economic losses and causes severe environmental pollution.[6–8] Consequently, the pursuit of effective methodologies to alleviate corrosion stands as a pivotal domain in scientific research, presenting an urgent imperative within the engineering discipline. To prevent the infiltration of corrosive agents into metals and the formation of microcells, measures can be instituted to decelerate and arrest this process, thereby realizing the objective of robust corrosion resistance efficiently. Polymer coating technology can provide protection and decoration for metals,[9] while metal plating technology, such as thermal spraying,[10] cold spraying,[11] chemical plating,[12] and electroplating,[13] can form firmly adhered coatings on metal surfaces to enhance performance. Chemical conversion technology, including chromate conversion films,[14] phosphate conversion films,[15] and rare earth salt conversion films,[16] can improve corrosion resistance through chemical reactions with metal surfaces. Anodic oxidation and micro-arc oxidation technology are also applicable to light metals like magnesium and aluminum,[17,18] forming dense oxidation layers to increase surface hardness and abrasion resistance. The application of these technologies can result in enhanced durability, corrosion resistance, and aesthetic qualities for metal materials. Nevertheless, these coating technologies exhibit certain drawbacks, such as environmental considerations, heightened surface hydrophilicity, and constrained protective functionalities. In response to these challenges, researchers are actively engaged in the exploration and development of novel technologies aimed at augmenting the multifunctionality, intelligence, and overall performance of protective coatings for metals.

Feng Chen

Prof. Feng Chen is a full professor of Electronic Engineering at Xi'an Jiaotong University, where he directs Ultrafast Photonic Laboratory (UPL), and has served as the director of Shaanxi key laboratory of Photonics Technology of Informtion (PTI) and the deputy director of the International Joint Research Center for Micro/Nano Manufacturing and Measurement Technologies. His current research interests are femtosecond laser microfabrication, bionic microfabrication and ultrafast photonics. Prof. Chen has published over 300 peer-reviewed papers in journals including Chem. Soc. Rev., Adv. Funct. Mater., Phys. Rev. Lett., etc.

The intricate and dynamic ecological environment imposes rigorous selection and adaptation challenges on all natural organisms. In response, a diverse array of creatures have evolved optimal structures and functions tailored to their surroundings. For example, lotus leaves are renowned for their capacity to repel dirt and water, known as the lotus leaf effect. Butterflies, through the flapping of their wings, disperse water droplets radially, preventing them from wetting the butterfly's body. Geckos exhibit swift wall maneuverability due to their highly adhesive feet. Mosquitoes maintain exceptional visual acuity even in foggy and dark conditions. Fish scales demonstrate effective self-cleaning and drag-reduction properties under water. By scrutinizing and emulating the structures and characteristics of these organisms, researchers are actively exploring the realm of biomimetic intelligent materials that integrate both structure and function. This avenue of investigation stands at the forefront of scientific exploration. The rapid progress in bionics holds promise for addressing and preventing metal corrosion. Materials and coatings inspired by bionics principles offer innovative concepts and avenues to achieve diverse functions, intelligence, and high performance in metal protective surfaces.

Bio-inspired anticorrosion strategies are crafted by drawing inspiration from the shapes, functions, and other elements observed in nature to address intricate corrosion challenges. For instance, emulating biological tissues with self-healing properties facilitates the active repair of coatings following breakage. The replication of plant leaves possessing water-repellent properties leads to the development of inert coatings that minimize contact with the external environment. Furthermore, diverse organisms in nature have evolved various protective mechanisms to achieve effective anti-biofouling. Fig. 1 illustrates the escalating trend in publications focusing on bio-inspired anticorrosion strategies from 2014 to 2023. This trend signifies the growing interest among scholars over the past decade, highlighting the increasing attention directed toward these strategies.

Several review articles offer intriguing summaries and analyses of existing scientific research on bionic surfaces for anticorrosion.[19–24] However, there is a relative scarcity of comprehensive overviews detailing the various types of bionic surface technologies. Particularly lacking are compilation and summarization of the corrosion prevention mechanisms, challenges, and response strategies associated with bionic surfaces developed in recent years. Biomimicry offers innovative solutions for preventing corrosion by emulating the structures and functions found in nature. Inspired by biological skin, researchers have created corrosion-resistant coatings with self-healing capabilities, reducing the incidence of corrosion. Morphological optimization, achieved through mimicking the structural forms of living organisms, facilitates the design of corrosion-resistant materials better suited to environmental conditions. For example, a coating with superhydrophobic properties has been developed by drawing inspiration from the surface texture of lotus leaves. This coating effectively prevents the adhesion of pollutants and corrosion of alloys. Despite the significant strides made in biomimetic strategies

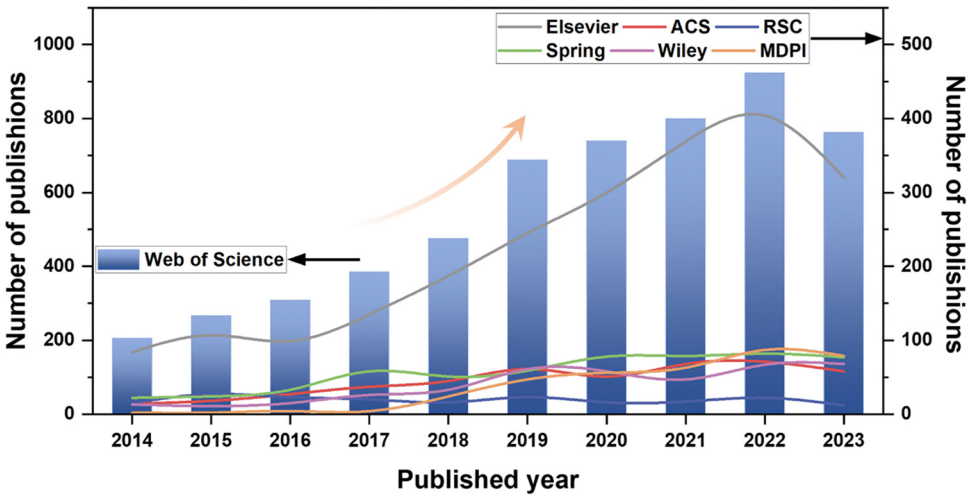

Fig. 1 The number of publications that concern bioinspired anticorrosion studies, each year from 2014 to 2023 [search in Web of Science, search words: corrosion (Topic) or anticorrosion (Topic) and bioinspired (Title) or biomimetic (Title) and nature-inspired (Title)].

for corrosion prevention, challenges such as the feasibility and cost of practical applications persist. This review addresses this gap by presenting three nature-inspired anti-corrosion strategies, as shown in Fig. 2. These strategies encompass biomimetic self-healing coatings that emulate biological tissues, biomimetic superhydrophobic surfaces exemplified by lotus leaves, and biomimetic slippery lubricant-infused porous surfaces inspired by the exceptional liquid repellency of Nepenthes. This review further provides a summary of their relevant technologies, anti-corrosion mechanisms, and applications. Additionally, it organizes the challenges and research advances in anti-corrosion coatings witnessed in recent years.

Biomimetic self-healing coatings

In the realm of nature, biological tissues exhibit remarkable adaptive capabilities to their external surroundings. These tissues effectively fulfill their biological functions even in challenging climates. Organisms, through a self-repair mechanism, possess the capacity to mend injuries inflicted upon them by the external environment. This reparative process aims to restore the original functionality of the wounded area, thereby ensuring the organism's optimal functioning and longevity. As an illustration, in the event of a skin injury, the blood emanating from the affected area carries coagulation factors,[25] initiating an automatic hemostatic response to halt bleeding. Concurrently, the injury to the skin triggers cell division and proliferation in the vicinity of the wound. This cellular activity is aimed at repairing the damaged skin and reinstating its original protective function.[26] It has become a hot research direction to imitate the self-healing ability of organisms and develop intelligent bionic materials that integrate sensing and driving and have good adaptive capacity to the external environment. Inspired by this, developing an anti-corrosion coating with a self-healing function to realize the active repair of a damaged layer is of great significance to extend the service life of the layer and reduce the maintenance cost. The definition of the self-healing function of the coating in the coating protection is different from that of the traditional self-healing function. In the classical understanding of the self-healing function, the self-healing function of a material requires the material to completely repair the damaged area and fully restore its original function. However, the most essential function of the anti-corrosion coating is to protect the base material from further damage by the surrounding corrosive media. Therefore, the protective coating has a self-healing function because its primary function is protection. Thus, only the recovery of the protective function of the coating can be realized at the damaged part of the coating without realizing all its functions, including the complete recovery of the original appearance of the coating.[27] According to the different objects repaired by the coating, the self-healing coating can be divided into the defect healing type and the corrosion suppression type.

Defect healing type

Defect-healing coatings aim to restore the corrosion resistance of the coating by incorporating microcapsule-coated repair agents or utilizing the inherent physical and chemical attributes of the coating.

2.1.1. Multi-shelled microcapsules. White *et al.*[28] were the first to introduce microcapsule technology into material design and apply it to the development of smart materials with self-healing capabilities. This advancement has the potential to extend the service life of materials. Fig. 3 shows the design scheme and working principle of a smart self-healing material. A self-repair reagent monomer dicyclopentadiene (DCPD) was encapsulated in a urea–formaldehyde shell by situ polymerization, and the Grubbs catalyst, which can catalyze the polymerization of the DCPD monomer, was dispersed in the epoxy polymer matrix. When the epoxy polymer material ruptures, the microcapsule ruptures, releasing the DCPD monomer, which acts as a self-repairing reagent and undergoes a polymerization

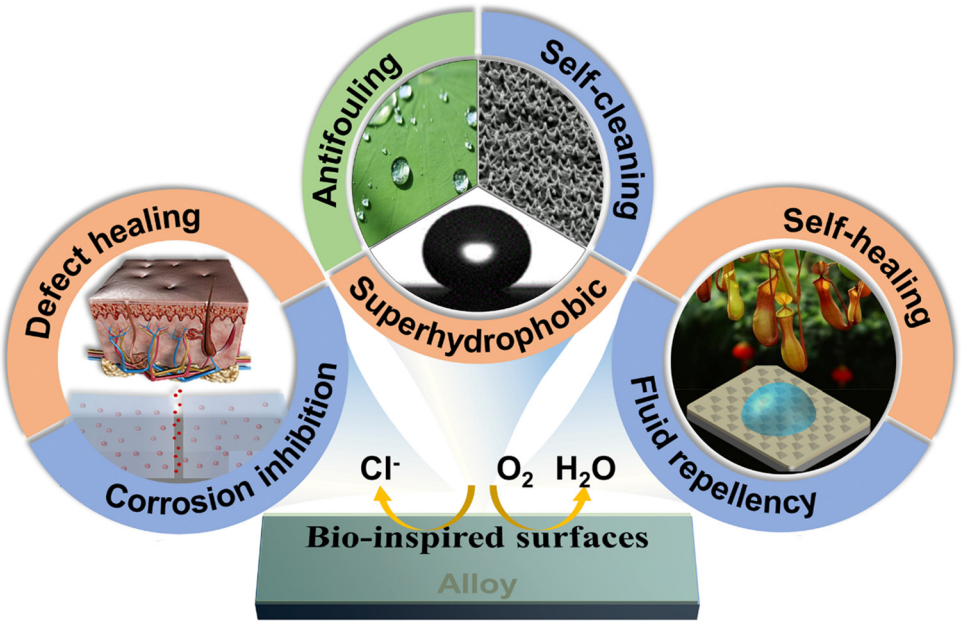

Fig. 2 A graphical abstract of bio-inspired anti-corrosion surfaces, including biomimetic self-healing coatings, biomimetic superhydrophobic surfaces, and biomimetic slippery liquid-infused porous surfaces.

reaction catalyzed by the Grubbs catalyst in the matrix, thus repairing the rupture in the material. However, Grubbs catalysts are expensive, and the self-repairing reagents released upon rupture of the microcapsules depend on the catalyst dispersed in the polymer matrix material for the curing process. If the catalyst undergoes structural changes leading to the loss of its catalytic properties, for example, because of poor thermal stability, the self-repair reagent cannot be cured, leading to the loss of self-repair function. Therefore, the development of catalyst-free, self-healing core materials can expand the range of applications for self-healing materials and avoid the effects of catalyst failure. One-component self-healing systems without the aid of catalysts and curing agents, represented by dry oils,[29–31] isocyanates,[32–34] and active silicones,[35–37] have been rapidly developed. The molecular structure of the repair agent of this system usually contains active functional groups that can polymerize under the action of O_2, H_2O, or light to realize the repair of coating defects and show good self-repair and corrosion resistance. For instance, Wang *et al.*[38] synthesized isocyanate microcapsules with isophorone diisocyanate and hexamethylene diisocyanate (HDI) as functional additives. They were used as potential healing materials for the water-triggered process by utilizing the "water" in the corrosion process as a "trigger switch" for the repair process. When microcracks are generated, the isocyanate released from the rupture of the microcapsules undergoes a polymerization reaction at room temperature to bond the cracks, effectively preventing corrosion from occurring and prolonging the service life of the anticorrosion coating.

Furthermore, Wang *et al.*[39] used a low-volatile HDI biuret as a healing material to prepare HDI biuret microcapsules by *in situ* polymerization instead of isocyanate, which is unfavorable to human health, and the study showed that it has an obvious self-healing effect under the trigger of water immersion,

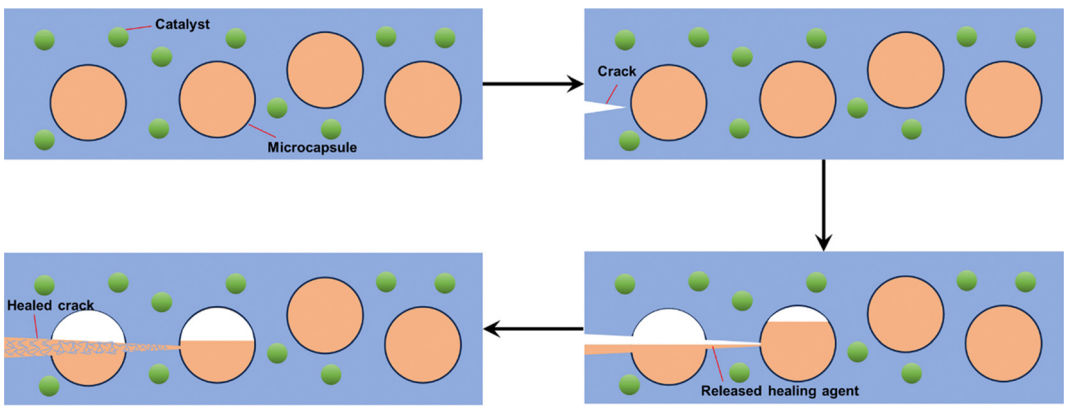

Fig. 3 A microencapsulated healing agent is embedded in a structural composite matrix containing a catalyst capable of polymerizing the healing agent.

which strengthened the corrosion protection of the damaged area of the coating. Feng *et al.*[40] prepared tung oil-loaded polyurethane (PU) microcapsules by interfacial polymerization and obtained tung oil-loaded PU/PANI double-shell microcapsules by *in situ* deposition of polyaniline (PANI) in a SiO_2-stabilized Pickering emulsion system. The synergistic effect of the tung oil core and the polyaniline wall, through the formation of a self-healing film and a passivation layer, resulted in a coating with excellent self-healing and anti-corrosion properties.

Microcapsule preparation technology has reached a level of maturity and diversity, making it easily combinable with coating materials. Consequently, the design space for a microcapsule-embedded self-healing coating system is expansive, holding significant promise for widespread applications. While polymer self-repair materials based on microcapsules can accomplish the self-repair function of coatings, the loading capacity of microcapsules in the material is relatively limited. This constraint results in the material's ability to execute a one-time self-repair function at the point of rupture. Subsequent damage to the coating poses challenges as the self-repair reagents within the microcapsules become depleted, hindering the ability to sustain further repairs.

2.1.2. Microvascular networks. It is necessary to supply a substantial amount of self-healing reagents continuously to address the challenge of multiple self-healing functions at the same break, ensuring a constant flow into the material break.[41] Upon damage to the coating caused by external forces, the interwoven microvessel network becomes compromised. The self-repairing reagent is released from the damaged section of the microvessel network, initiating further curing and other reactions at the affected site. This autonomous repair process can be iteratively repeated numerous times. The construction of one-dimensional tubular structures in polymers is feasible through the utilization of hollow fibers, microtubes, or microchannels.[42–45] With more sophisticated designs, a three-dimensional microvessel network embedded in the polymer becomes capable of transporting two-component self-healing reagents (Fig. 4). Hansen *et al.*[46] demonstrated that dual-vessel-based self-healing composites are capable of achieving more than 30 repetitions of self-healing through their study. In addition, Hansen *et al.*[47] suggested that the temperature and time of self-repair can be theoretically regulated by introducing a third independent microvessel network function, allowing the material to self-repair in harsh environments as well.

Despite the numerous advantages of self-repairing materials with microvascular network systems, several challenges must be addressed before practical applications. In the production and preparation process, efforts should be made to reduce the cost associated with microvessel network-based self-repair materials.[48] Additionally, when designing such materials, special attention is required to ensure that the intelligent self-repair features do not compromise or adversely impact the properties and functions of the substrate material, which includes addressing concerns related to the circulation of self-repair reagents in microvessels and ensuring the feasibility of multiple self-repair processes.

Damage at the millimeter scale poses a challenge for a single self-healing material system to repair multiple scales of material damage simultaneously. Hence, the integration of multiple self-healing strategies can be employed in the design of self-healing materials. Gergely *et al.*[49] designed a self-repairing material using both microcapsule and microvessel strategies, which is capable of autonomously repairing damage within the micrometer scale and millimeter scale at the same time. The

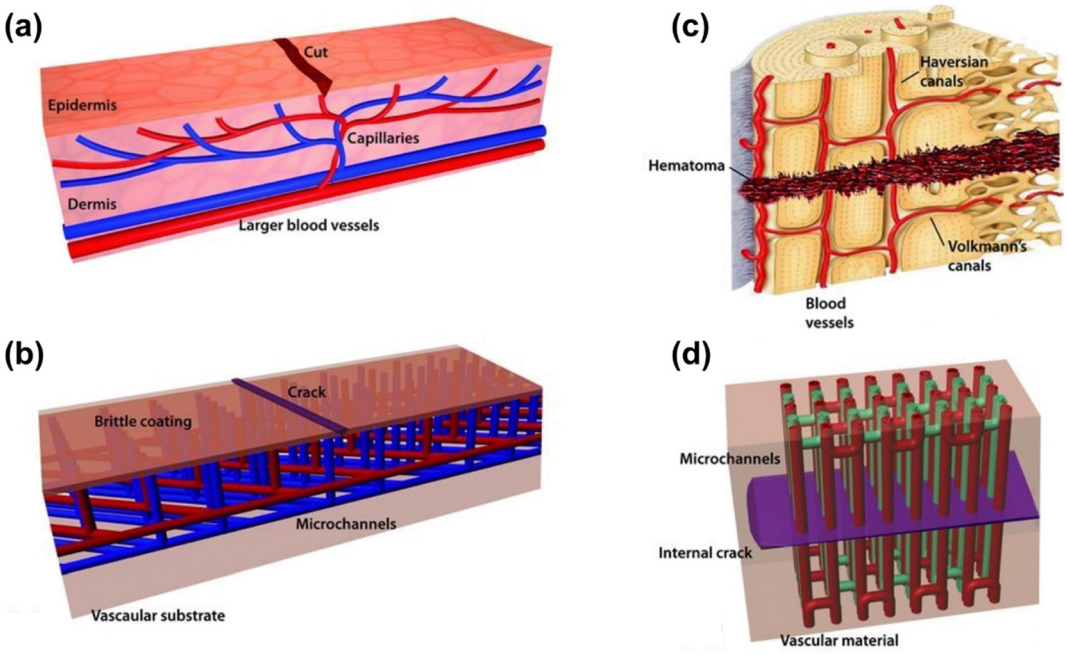

Fig. 4 Schematic diagram of a microvascular structure (reproduced from ref. 41 with permission from [Wiley], copyright [2010]).

microvessel network was used to deliver repair reagents with two-stage reaction characteristics to repair large-size damage due to punctures in the system. In contrast, microcapsules loaded with epoxy monomer-based self-repair reagents were used to repair damage such as microcracks generated. By adjusting the monomer self-repair reagent, the strength of the material after curing can be between 1.1 MPa and 1.4 GPa, thus ensuring that the strength of the material after the completion of self-repair at the damage is close to the strength of the material before damage. The experimental results show that the self-repair system with microcapsule-microvessel hybridization not only enables the self-repair efficiency of the matrix material to reach 100% but also enables the simultaneous repair of microcracks in the matrix material due to the microcapsule system, realizing the complete restoration of the morphology of the matrix material.

2.1.3. Core–shell nano- and micro-fibers. Recent studies have identified core–shell structural epoxy coatings as an effective self-healing technique, providing a cost-effective alternative to microencapsulation.[50] Nanofibers are popular due to their excellent mechanical and thermal properties combined with high porosity and large surface area to volume ratio. These characteristics contribute to the homogeneous dispersion of healing carriers in composites and ensure a benign interaction with the matrix and reinforcing fibers, preventing disruption to their surface morphology. Electrostatic spinning technology is commonly employed for fiber production. Sinha-Ray *et al.*[51] pioneered the use of micro/nanofibers as a self-healing carrier, employing polyacrylonitrile (PAN) as the shell and encapsulating DCPD and isophorone diisocyanate *via* the electrostatic spinning technique. Wang *et al.*[52] encapsulated self-healing epoxy resin and a curing agent in polyacrylonitrile by coaxial electrostatic spinning to form two-component core–shell nanofibers. The healing efficiency could reach 110.12% after self-healing for 1 h at 120 °C. Mao *et al.*[53] synthesized PAN nanocore-shell fibers using the electrostatic spinning technique and incorporated them into a carbon fiber-reinforced polymer. The addition of core–shell nanofibers enabled the material to self-heal to 80% of its undamaged residual compressive strength when subjected to impacts with energies lower than 37.5 J.

Beyond the electrostatic spinning method, Lee *et al.*[54] were the first to utilize commercial epoxy resins as healing agents embedded in nanofibers and microfibers formed through solution blow molding. Remarkably, this method has been successfully scaled up to an industrial level and is at least 30 times faster than the electrostatic spinning process.

2.1.4. Intrinsic self-healing materials. Intrinsic-type materials can be designed through various mechanisms, including thermally reversible chemical reactions, ammonia bonding, ionomer rearrangements, diffusion and entanglement of molecular-level polymer chain segments, coordination chemistry, and host–guest interactions. Intrinsic materials possess a unique ability to self-heal at the molecular level, making them the closest to an ideal material compared to external additives like microcapsules or microvessels. In self-healing polymers relying on reversible Diels–Alder dynamic chemical reactions, thermally reversible covalent bonding facilitates the dynamic exchange of covalent bonds within the material when heated. This process effectively repairs microcracks that may occur in the material.[55–57] The self-healing function is more readily achievable in thermoplastic polymers, primarily because they are linear polymers with polymer chain segments that exhibit greater mobility compared to thermoset polymers.[58] Consequently, when thermoplastic polymers are subjected to heat, the polymer chain segments at the rupture interface can come into contact and entangle, effectively realizing the self-healing capability of the material. However, it is important to note that thermoplastic polymers generally exhibit lower mechanical strength. In contrast, thermosets possess a crosslinked network structure, resulting in higher mechanical strength.[59] However, the presence of these crosslinked networks makes thermosets challenging to reuse multiple times. When compared to thermally reversible self-healing coatings, photoplastic self-healing coatings offer the advantage of remote and precise repair of damaged areas. This characteristic helps minimize the side effects of the self-healing process and reduce the risk of thermal damage to intact areas of the coating.[60]

Dopamine chemistry is a recently developed biomimetic chemical means in which the presence of the o-phenol hydroxyl group makes the dopamine-based materials have excellent bonding properties and self-repairing properties even under water,[61] and the dopamine-based materials do not need any other stimulation to achieve rapid and efficient self-repairing properties of their materials.[62–64] However, the small bond energy of dynamic non-covalent bonding leads to weak mechanical properties of self-healing materials prepared by dynamic bonding, which limits their further applications. Therefore, improving the mechanical properties of dynamic non-covalent bonded self-healing materials has become an important direction in the research of this class of self-healing materials. The mechanical properties of the self-healing materials were effectively enhanced by using inorganic materials for toughening, carbon materials, and the introduction of a dual network structure.[65–67] Natural organisms exhibit remarkable self-healing abilities coupled with extraordinary mechanical strength, prompting researchers to delve into the structure and functions of these organisms. This exploration proves to be a highly rewarding endeavor. In the realm of biomimicry, the focus extends beyond mere imitation of a living organism's structure; it involves integrating structure and function to develop new materials that either replicate or surpass the structural attributes of the original organism. For instance, biological tissues like skin, with their layered structure, resilient bones, and the sturdy shells of mollusks, possess the capability to undergo complete self-repair following damage through a series of coordinated chemical and physical processes. Over hundreds of millions of years of natural evolution, these biological tissues have not only achieved structural excellence but have also optimized the repair process, maximizing resource and energy efficiency. Consequently, the development of materials that mirror the efficiency and environmental friendliness of biological tissues, coupled with high-strength self-repair capabilities, emerges as both a challenging

task and an urgent priority in the domains of corrosion prevention and self-repair materials.

2.2. Corrosion inhibition type

In contrast to defect-healing self-healing coatings, corrosion-inhibiting self-healing coatings employ an alternative approach by impeding metal corrosion through the incorporation of an active substance into the coating.

2.2.1. Nanocontainers. Direct doping of corrosion inhibitors into the coating poses challenges in achieving controlled release, potentially leading to the rapid depletion of the corrosion inhibitor over a short period. Moreover, there is a risk of the corrosion inhibitor reacting with certain components of the coating matrix, resulting in issues such as corrosion inhibitor failure or degradation of coating performance. In contrast, encapsulating the corrosion inhibitor in a nanocontainer before dispersing it into the coating provides an effective solution by isolating the corrosion inhibitor from the coating substrate. The presence of nanocontainers not only prevents direct contact between the corrosion inhibitor and the coating but also imparts a certain environmental responsiveness to the corrosion inhibitor, which allows controlled release and migration of the corrosion inhibitor to the corrosion site under external stimuli, such as a magnetic field, temperature, light, or pH. Subsequently, the released corrosion inhibitor can inhibit the electrochemical activity of the corrosion site through processes like adsorption, passivation, or chelating reactions with metal ions. This mechanism helps block the further expansion of corrosion.

Porous materials characterized by a high specific surface area serve as excellent candidates for nanocontainers loaded with corrosion inhibitors. Table 1 provides an overview of the research progress in nanocontainers based on corrosion inhibitors for the development of self-healing coatings.

Inorganic nanocontainers predominantly consist of mesoporous nanoparticles like SiO_2, TiO_2, and CeO_2, among others. The anti-corrosion mechanism typically involves loading the cavities of inorganic nanoparticles with both inorganic and organic corrosion inhibitors. The release of corrosion inhibitors is controlled in response to environmental stimuli, coupled with physical or chemical actions on the metal surface, thereby preventing corrosion. For instance, Habib *et al.*[71] utilized ZrO_2 nanoparticles as carriers loaded with a self-repairing agent polyethyleneimine (PEI) and a corrosion inhibitor imidazole (IM). Prolonged electrochemical tests in a 3.5 wt% NaCl solution demonstrated excellent corrosion resistance in the epoxy-based bilayer nanocomposite coatings after a 7-day immersion in the corrosive medium. Khan *et al.*[75] incorporated a corrosion inhibitor IM into halloysite nanotubes (HNTs) and coated the surface with a polyelectrolyte multilayer film consisting of PEI and sulfonated polyether ether ketone, with insertion of dodecyl amine (DDA). Electrochemical impedance spectroscopy (EIS) tests revealed corrosion inhibition efficiencies of 92% and 99.8% for the modified and hybrid coatings, respectively.

HNTs are natural silica-aluminate nanomaterials with a versatile application scope in the field of anticorrosive coatings owing to their distinctive hollow tubular structure. However, the inherent corrosion inhibitor loading efficiency of pristine HNTs is relatively low. Many studies have employed sulfuric acid to etch HNTs, creating hybrid halloysite nanotubes as a smart carrier. This process increases pore volume and enhances loading efficiency. Nonetheless, the sulfuric acid treatment poses a risk of damaging or partially decomposing the hollow tubular structure of HNTs. In a recent study, Zhao *et al.*[84] opted for a milder approach using acetic acid to etch HNTs, aiming to enhance the loading capacity of the corrosion inhibitor methyl benzotriazole (BTA). The loading of BTA increased from 1.57 wt% to 2.33 wt%. Notably, the authors applied polydopamine (PDA) to coat the HNTs, improving their dispersion in the epoxy resin and effectively reducing the release of BTA in the absence of corrosion.

Organic nanocontainers have been extensively utilized in the formulation and investigation of corrosion inhibitor coatings, primarily owing to their cost-effectiveness, straightforward synthesis, and high specific surface area. The corrosion prevention mechanism inherent in organic nanocontainers closely parallels that observed in inorganic nanocontainers. Drawing inspiration from mussel adhesive proteins, Shen *et al.*[85] synthesized HNQ-EN *via* a Schiff base reaction involving 5-hydroxy-1,4-naphthalenedione (HNQ) and ethylenediamine (EN). The

Table 1 Summary of nanocontainers for self-heal coating

Group	Type	Corrosion inhibitor	Applied coating	Substrate	Ref.
Inorganic nanocontainers	SiO_2	2-Aminino-5-mercato-1, 3,4-thiadizole, BTA	Epoxy	Copper, aluminum alloy	68 and 69
	TiO_2	Molybdate	Polypyrrole	304 stainless steel	70
	ZrO_2	IM	Epoxy	Carbon steel	71
	CeO_2	BTA, dodecylamine, *n*-methylthiourea	Silane-based coating, epoxy	Copper, carbon steel	72 and 73
	Talc nanoparticles	$NaNO_3$	Epoxy	Carbon steel	74
	HNTs	IM	Epoxy	Carbon steel	75
	NaY zeolite	BTA	Epoxy	Q235 low-carbon steel	76
	Graphene oxide (GO)	BTA, 2-mercaptobenzothiazole	Epoxy	Q235 carbon steel	77
	MWCNT	Polyaniline, Zn^{2+}	Epoxy	Mild steel	78
Organic nanocontainers	Cyclodextrin	Dopamine	Silane-based coating	Steel	79
	Polydopamine	Zn^{2+}	Epoxy	Mild steel	80
	Polyvinyl butyral	Gallic acid and phenanthroline	Epoxy	Q235 steel	81
	Urea-formaldehyde	Fluorinated alkyl silane	Epoxy	Q235 steel	82
Organic–inorganic hybrids	ZIF-8	Glutamate molecules, Zn^{2+}	Epoxy	ST12-grade low-carbon steel	83

resultant HNQ-EN is subsequently combined with $Ti_3C_2T_x$, denoted as HE-$Ti_3C_2T_x$, functioning as a nanocontainer for cerium nitrate. This unique combination imparts self-healing properties to the epoxy coating. Experimental outcomes demonstrated a substantial enhancement in inhibition efficiency, increasing from the initial 7.8% to an impressive 91.1% after subjecting the samples to immersion in a 3.5 wt% NaCl solution for 36 hours.

2.2.2. Layer-by-layer coating technique. The layer-by-layer (LBL) coating technique stands out as a versatile, cost-effective, relatively simple, and easily scalable method for the production of intelligent capsules with potential applicability in large-scale industrialized production. In a study reported by Chen *et al.*,[86] the LBL method was employed to fabricate a novel pH-sensitive SnO_2 nanocontainer. The process involved depositing a polypyridine layer onto SnO_2 nanoparticles, synthesized through a hydrothermal method using *in situ* chemical polymerization. Subsequently, ultrasonic loading of the Na_2MoO_4 layer and stirring resulted in the acquisition of a PDA-modified nanocontainer. The incorporation of a polydopamine (PDA) outer layer exerted control over the on-demand release of the molybdate corrosion inhibitor, simultaneously modifying the cracked polymer network through the utilization of dopamine functional groups and iron oxide. This enhancement significantly bolstered the self-healing capability of the epoxy coating, showcasing commendable corrosion resistance. In a separate study, Fathabadi *et al.*[87] synthesized intelligent multilayer pH-sensitive nanocapsules using the LBL strategy. The outer shell comprised multilayered polystyrenesulfonate (PSS)/PEI/PSS, while the inner shell consisted of PSS/cetyl trimethyl ammonium bromide (CTAB). ZrO_2 was loaded with the corrosion inhibitor tolyltriazole, as illustrated in Fig. 5. The nanocapsules exhibited automatic release of the loaded corrosion inhibitor, providing surface protection under both strongly acidic and alkaline conditions.

The integration of corrosion inhibitor loading techniques with emerging technologies, such as shape memory technology, has led to a rapid development of synergistic approaches to enhance various repair mechanisms. Li *et al.*[88] explored the feasibility of depositing a SiO_2/BTA/graphene quantum dot (GQD) coating on PDA (PSBG) as an effective LBL system for self-healing shape memory polymer (SMP) coatings on the AA2023 aluminum alloy. The remarkable passive and active corrosion protection capabilities of the PSBG can be delineated in three key aspects. The first key mechanism involves the PSBG composite nanofillers, which possess a robust photothermal conversion capability. This capability significantly facilitates the melting of Brazilian carnauba wax particles. This process serves a dual purpose: repairing coating defects and activating the occlusion effect within the SMP coating. The second mechanism operates at elevated temperatures, where the hydrogen bonding between the GQD cap and the polymeric shape (PS) container is disrupted. This disruption allows BTA to actively self-release, providing an additional layer of protection to the alloy. The final mechanism focuses on the enhanced corrosion resistance of the repaired PSBG-based coatings. This improvement is attributed to the presence of functional groups on the surface of GQDs, which contribute to the improved dispersion and compatibility of nanofillers within the SMP coatings.

3. Biomimetic superhydrophobic surfaces

Nature, over an extensive process of evolution, has bestowed various organisms with microscopically intricate structures,

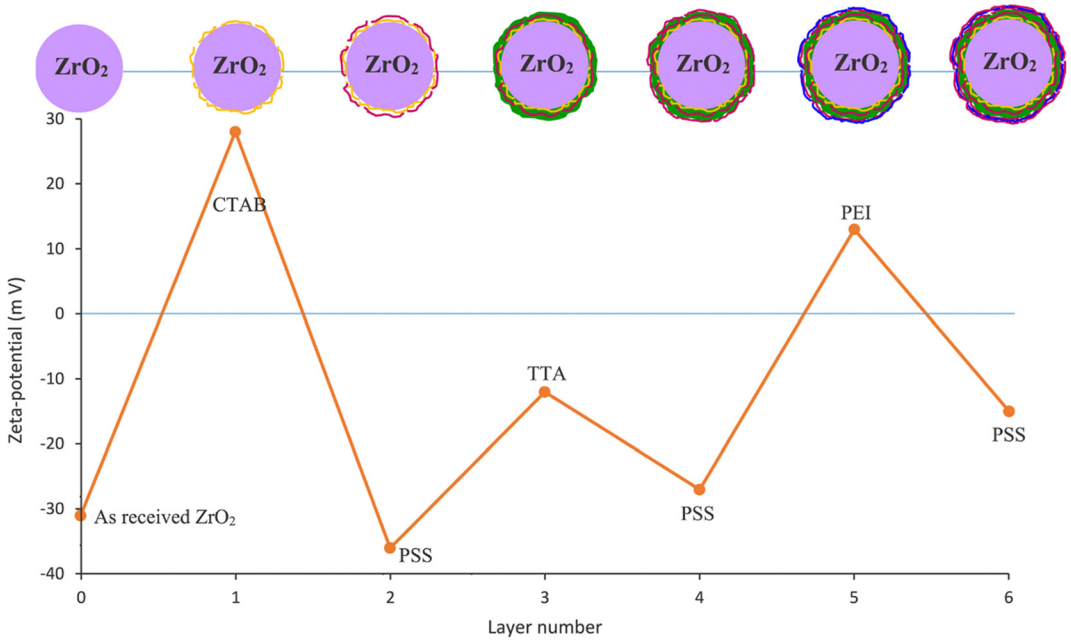

Fig. 5 Zeta-potential measurement of ZrO_2 nanoparticles and obtained compounds after each stage of the LBL process (reproduced from ref. 87 with permission from [Elsevier], copyright [2021]).

leading to the manifestation of captivating phenomena on a macroscopic scale. Notable examples include rose petals exhibiting dazzling color refraction in daylight when adorned with water droplets, a spectacle attributed to the structural intricacies of micron-sized bumps and nanometer-sized folds on the petal surface. Similarly, the enchanting sight of a butterfly fluttering in the rain is achieved through the combination of micron-sized scales and nanometer-sized grooves on the wing surface. In contrast, lotus leaves, growing in silt without staining, owe their hydrophobic nature to the micro- and nano-scale raised structures on their surfaces, as shown in Fig. 6. Inspired by these naturally occurring superhydrophobic phenomena, researchers have successfully enhanced corrosion resistance by introducing texture and reducing surface energy on metal or alloy substrates.[89–92] Pioneering work reported by Liu *et al.*[93] marked the first utilization of superhydrophobic surfaces (SHSs) for copper corrosion protection in seawater. They developed a superhydrophobic membrane covering the copper surface through an *n*-tetradecanoic acid etching process. EIS results unequivocally confirmed the outstanding corrosion resistance conferred by the membrane. The researchers highlighted that a synergistic effect of air-trapped valleys and capillary forces contributes significantly to the bolstered corrosion resistance. As research on SHSs for metal corrosion protection continues to expand, these coatings emerge as an effective strategy to combat metal corrosion in highly aggressive environments.

3.1. Theoretical modeling of surface wettability

Wettability is one of the physicochemical properties of a solid surface and is expressed as the tendency of a liquid to diffuse to varying degrees on a solid surface. The contact angle of a liquid on a solid surface is the angle θ between the tangent of the gas–liquid interface at the gas–liquid–solid three-phase boundary and the solid–liquid interface on the liquid side (Fig. 7(a)). The sliding angle is defined as the critical angle formed between the solid surface and the horizontal plane when a liquid droplet precisely begins to roll on the solid surface. Both the contact angle and sliding angle are commonly employed parameters for characterizing the surface-wetting properties of materials. The wettability of a solid surface is intricately linked to interactions at the solid/liquid/gas interface. Notably, superhydrophobic surfaces stand out in the realm of wettability, typically showcasing a contact angle greater than 150° and a sliding angle less than 10°. These specific characteristics highlight the remarkable water-repellent nature of superhydrophobic surfaces, making them highly effective in resisting liquid contact and facilitating self-cleaning properties.

To investigate the wettability characteristics of sample surfaces, researchers have developed and optimized wettability models for materials. In the case of an ideal solid substrate that is perfectly flat and chemically homogeneous, when a droplet is deposited on the solid surface, it initiates contact with the substrate, forming a three-phase contact line. The determination of the contact angle of the sample primarily relies on the surface energy and surface tension at the solid–gas, liquid–gas, and liquid–solid interfaces. This relationship is encapsulated in Young's equation:

$$\gamma_{ls} - \gamma_{sg} + \gamma_{lg}\cos\theta = 0 \quad (1)$$

Here, γ_{ls}, γ_{sg}, and γ_{lg} represent the surface tension of the liquid–solid, solid–gas, and liquid–gas interfaces, respectively. This equation can also be alternatively expressed as:

$$\cos\theta = \frac{\gamma_{sg} - \gamma_{sl}}{\gamma_{lg}} \quad (2)$$

Since the equation characterizes the contact angle of a droplet on a perfectly smooth ideal plane, the contact angle is also the intrinsic contact angle of the material. These equations encapsulate the fundamental relationship governing the contact angle of a droplet on an ideal solid substrate and are instrumental in the study of wettability characteristics on different surfaces.

Certainly, the condition for non-wettability of a solid surface often involves the presence of a rough structure. In such cases, the actual surface area of a rough substrate exceeds its apparent surface area. Wenzel introduced a new model to describe the contact angle on a rough surface, building upon Young's model. The relationship between the actual contact angle (θ_w) and the intrinsic contact angle (θ_s) of a droplet on a material surface is expressed as follows:

$$\cos\theta_w = r\cos\theta_s \quad (3)$$

Here, r represents the roughness factor. In this state, the droplets wet the surface and fill the rough surface voids (Fig. 7(b)). In Wenzel's equation, when the solid surface θ_s is less than 90°, θ_w decreases with the increase of r, which favors the wet contact between the droplet and the surface. When the solid surface θ_s is greater than 90°, θ_w increases with the increase of r, and the hydrophobicity of the surface is

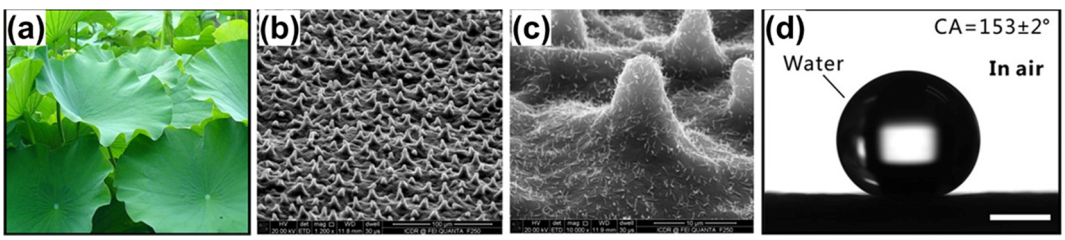

Fig. 6 Superhydrophobicity of lotus leaves. (a) Photograph of lotus leaves, (b) and (c) surface microstructures on lotus leaves, (d) water droplets on lotus leaves in air (reproduced from ref. 94 with permission from [American Chemical Society], copyright [2017]).

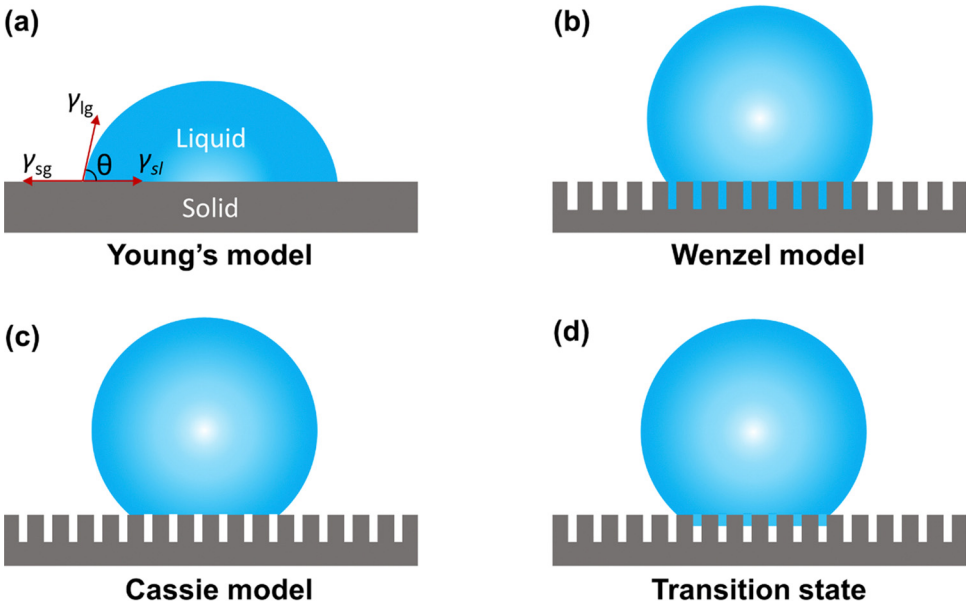

Fig. 7 Typical wetting behavior of a droplet on a solid surface. (a) Young's model, (b) Wenzel model, (c) Cassie model, and (d) transition state.

enhanced. When r of the hydrophobic surface is large, the penetration of the droplet will be hindered by the air trapped in the rough structure, and it is difficult to realize the wet contact between the droplet and the surface. Wenzel's equation is not suitable to explain this phenomenon.

The Cassie model presents a framework for elucidating the contact angle of droplets on the surface of an inhomogeneous material. In this model, water droplets adhere to a rough structure on a solid surface, comprising an air layer instead of directly wetting the surface, as illustrated in Fig. 7(c). By introducing the contact area fraction f_1 between water droplets and the rough structure and the contact area fraction f_2 between water droplets and air trapped in the rough structure ($f_1 + f_2 = 1$), the Cassie equation can be expressed as:

$$\cos\theta_C = f_1 \cos\theta_s + f_2 \cos\theta_g \quad (4)$$

Here, θ_C is the apparent contact angle of the droplet in the Cassie state, and θ_g is the contact angle of the droplet on the air surface. Given that the contact angle of the droplet with air is 180°, eqn (4) can be formulated as follows:

$$\cos\theta_C = rf_1 \cos\theta_s + f_1 - 1 \quad (5)$$

When $f_1 = 1$, the Cassie equation is transformed into the Wenzel equation. When a fraction of the liquid infiltrates between rough structures, the contact state of the droplet lies between the Wenzel state and the Cassie state. This contact model is commonly referred to as the "transition state" or the "intermediate state," as depicted in Fig. 7(d). Therefore, it is essential to ensure the sustained stability of the surface state to maintain the Cassie state consistently.

3.2. Anti-corrosion mechanisms on superhydrophobic surfaces

Metal corrosion occurs under specific conditions, which include the presence of active corrosion sites serving as both the anode and cathode, electrical contact, a continuous electrolyte phase between the anode and cathode, and, finally, the existence of a cathodic reaction component capable of absorbing electrons produced through the ionization of the metal anode.[95] SHSs exhibit micron-nanometer-scale roughness and possess low surface energy. The indentations on the non-uniform surface facilitate the easy entrapment of air. Consequently, corrosive substances, such as chloride ions, are effectively hindered by the air layer, preventing the degradation of the metal. With the growing research interest in superhydrophobic surfaces for metal corrosion prevention, scholars have discerned that the mechanism of SHS corrosion prevention extends beyond the mere isolation of the air layer. It also involves the synergistic impact of the hydrophobic agent layer, the textured structure, and the air layer.[96–98]

Regarding the hydrophobic agent layer, the hydrophobic molecules play a crucial role in preventing the adsorption of corrosive ions or molecular oxygen at the active corrosion sites (Fig. 8(a)). The hydrophobic agent forms an ordered chemisorption layer, acting as a barrier to charge transfer. Consequently, the hydrophobic molecular layer on the textured metal surface renders the metal less susceptible to corrosion. Furthermore, it influences the charging conditions at the interface where corrosion takes place. Metals/oxides typically carry a positive charge in neutral solutions, leading to the electrostatic attraction of aggressive anions. In contrast, hydrophobic materials exhibit a negative charge in a neutral solution, owing to their isoelectric point in the electrolyte at pH 2–4. The negative charge of the SHS results in an ion redistribution in the bilayer, diminishing the concentration of halide anions in the proximity of the solid surface (Fig. 8(b)).

In the context of the textured structure of SHSs, corrosion media are repelled from the surface grooves through capillary pressure within the microstructure, as depicted in Fig. 8(c). Certain preparation methods, such as laser ablation for

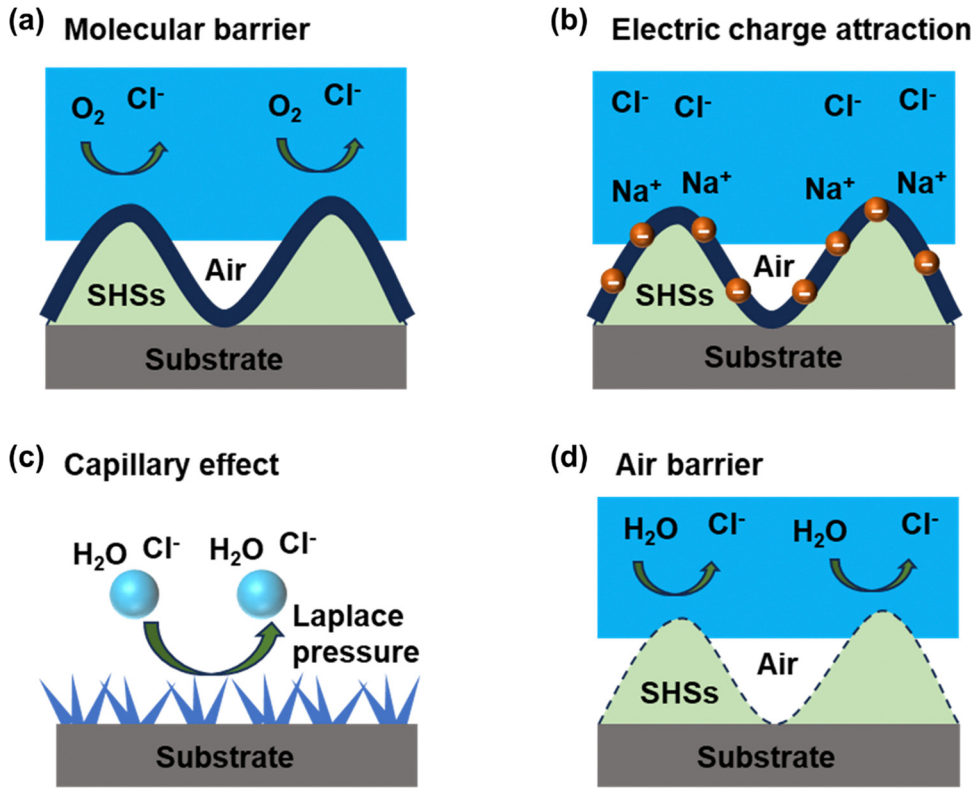

Fig. 8 Schematic diagram of the anti-corrosion mechanism on SHSs.

constructing the textured structure, yield an oxide surface layer with favorable properties for blocking charge, chloride ions, and water molecule transfer, thereby further impeding corrosion reactions. SHSs also exhibit a water contact angle exceeding 150° and low wetting hysteresis. These characteristics ensure that an aqueous medium wets the coating material in a non-uniform wetting state, retaining air in the grooves of the textured surface. The liquid only contacts the material on the surface of the protruding peaks, resulting in a significantly smaller true wetting area between the liquid and the material compared to the apparent contact area (Fig. 8(d)).

3.3. Design strategies for superhydrophobic surfaces

Many organisms have developed a variety of micro/nanostructured surfaces that display biological properties to survive under natural stresses. For example, micro/nanostructures such as lotus leaves,[98] shark skin,[99] and butterfly wings[100] endow each surface with excellent self-cleaning and degradable capabilities, allowing each organism to adapt to its surroundings. These natural strategies inspire the fabrication of artificial surfaces mimicking biological properties. The creation of biomimetic superhydrophobic surfaces typically involves two technological approaches: constructing micrometer and nanorough structures on the surface of hydrophobic materials with low surface energy or modifying rough structures with low surface energy on the micrometer and nanometer scales. Various fabrication methods have been employed to create micro/nanostructured surfaces, and when preparing biomimetic anti-corrosion surfaces, considerations extend beyond performance and functionality to include cost and technical difficulty. Table 2 provides a summary of commonly used methods for preparing superhydrophobic surfaces, outlining their advantages and disadvantages.

3.3.1. Spray/spin coating. The spray/spin coating method typically entails spraying a suspension of nanoparticles onto various substrates. This method is characterized by its simplicity, ease of implementation, and suitability for large-scale industrial production. Li *et al.*[116] employed a hybrid approach to prepare EP + PDMS@SiO_2 and uniformly sprayed it onto magnesium alloys. The results demonstrated a remarkable reduction in the corrosion current by two orders of magnitude compared to the initial state, showcasing superior corrosion resistance. Notably, the coating exhibited resistance to high-temperature fluids and demonstrated the ability to recover from storm leakage under low-temperature conditions.

Furthermore, it maintained superhydrophobic properties even after abrasion and tape stripping. In a similar vein, Shen *et al.*[117] achieved superhydrophobic F-SiO_2@PDMS coatings by initially spraying a PDMS layer on an aluminum alloy and subsequently applying a mixed solution of fluorinated silica and PDMS. The resulting non-wetting state, attributed to trapped air pockets, endowed the superhydrophobic F-SiO_2@PDMS coatings with excellent corrosion resistance. The electrochemical impedance modulus exhibited a notable increase of up to three orders of magnitude compared to the pure aluminum alloy.

Table 2 Methods commonly used to prepare SHSs and their advantages and disadvantages

Method	Advantage	Disadvantage	Ref.
Electrodeposition	Simple operation and low process cost	Poor bonding effect with the substrate	101–104
Chemical etching	Simple preparation process	Higher cost and environmentally unfriendly	105 and 106
Laser processing	Simple operation, high precision, and high efficiency	High cost	107–110
Spray/spin coating	Simple construction, high flexibility, and low cost	Waste raw materials	111–113
Sol–gel	Low cost and simple preparation	Poor durability	114 and 115

3.3.2. Electrodeposition. Electrodeposition is a widely employed technique for depositing superhydrophobic surfaces onto metallic substrates. In this process, the application of an electrical potential between two electrodes initiates the dissolution of metal ions at the anode into the electrolyte, while those at the cathode undergo reduction, resulting in the formation of a metallic coating on the substrate. The manipulation of surface morphology is achievable by adjusting various parameters. Electrodeposition stands out as a promising method for crafting micrometers and nanostructures owing to its inherent advantages of low cost and simplicity.

Mousavi *et al.*[118] prepared superhydrophobic surfaces on copper substrates using a distributed electrodeposition technique. The prepared surface has a water contact angle of more than 155° and exhibits excellent superhydrophobicity. The unique surface texture helps to trap large amounts of air and forms an air cushion underneath the water droplets, thus preventing the liquid from contacting the copper substrate. The superhydrophobic surface was shown to inhibit corrosion by two to four orders of magnitude compared to bare copper. Wang *et al.*[119] achieved the preparation of superhydrophobic nickel films on copper foils using a one-step electrodeposition method, incorporating choline chloride as a crystal modifier. The static contact angle of the nickel film reached 162° under optimal parameters. Notably, this method obviated the need for organic surface modification to attain superhydrophobic properties. The resulting samples exhibited remarkable protection, with a corrosion inhibition efficiency of 99.6%. While the protective properties gradually diminished with immersion in a corrosive medium, even after 15 days, the film retained a high corrosion inhibition efficiency of 89.84%.

The presence of a superhydrophobic coating in the Cassie state can be considered a barrier, thus providing a perfect gas–liquid interface that inhibits the penetration of corrosive ions. However, surfaces prepared by electrodeposition have poor durability and stability due to poor adhesion strength and fragile micro/nanostructures. Combining electrodeposition with other techniques by adding nanofillers, such as nanoparticles or nanofibers,[120–122] can enhance the mechanical strength and stability of superhydrophobic coatings.

3.3.3. Etching technique. Etching techniques utilized for the preparation of SHSs commonly involve chemical etching and laser texturing. The underlying principle is to enhance surface roughness by selectively removing substrate materials through either physical or chemical reactions. Chemical etching is a commonly used method that utilizes a strong acidic or alkaline solution to form micro/nanostructures. Dou *et al.*[123] successfully prepared superhydrophobic microneedle CuO surfaces on a copper surface using a simple chemical etching method and fluoride treatment. Based on the air-layer theory in the Cassie state, electrochemical tests showed that I_{corr} of the superhydrophobic samples was reduced by nearly three orders of magnitude compared with the untreated ones, providing excellent corrosion protection. However, chemical etching rates are difficult to control, and the etching reaction can be controlled and accelerated by adjusting the composition, concentration, or temperature of the etchant.

In recent years, laser processing has garnered significant attention from researchers due to its high efficiency, precision, and universality. Notably, femtosecond lasers, with ultrashort pulse times in the order of femtoseconds (10^{-15} s), possess a substantial peak power exceeding the damage threshold of most materials. This characteristic allows femtosecond lasers to process a wide range of materials, including metals, ceramics, polymers, and biomaterials, without significant limitations in material selection. Yong *et al.*[124] have outlined advancements in manipulating the wettability of materials through femtosecond laser processing. By designing and machining various microstructures on substrates, they achieved superhydrophobic properties, underwater superhydrophobic properties, anisotropic wettability, and intelligent wettability. Additionally, materials like PDMS and PTFE could attain superhydrophobic properties solely through femtosecond laser processing. The creation of micro-nano grooves on material surfaces enabled anisotropic wetting and droplet sliding, showcasing potential applications in droplet manipulation, microfluidics, biology, and other fields. Femtosecond laser technology has gained popularity for biomimetic applications due to its ability to mimic biological surface structures easily. In terms of corrosion resistance, the femtosecond laser process is adept at producing stable superhydrophobic coatings that exhibit strong water repellency, utilizing the formation of interfacial bubbles in the Cassie state. Moreover, Rajan *et al.*[125] delved into the laser-induced amorphization of metal surfaces, attributing it to the increase in crystal dislocation density caused by femtosecond laser-induced stress and compressive strain. This phenomenon plays a pivotal role in enhancing corrosion resistance by significantly reducing the free energy of amorphous materials, thereby increasing the chemical stability of metal alloys and reducing the reactivity of their elements.

3.3.4. Other methods. In addition to the previously mentioned methods, various approaches for preparing superhydrophobic materials include chemical vapor deposition (CVD), template methods, and electrostatic methods. Vilaró *et al.*[126]

etched the copper surface by alternating plasma to produce a layered structure and then deposited 1*H*,1*H*,2*H*,2*H*-perfluorodecyl acrylate-ethylene glycol diacrylate [*p*(PFDA-*co*-EGDA)] on top of the metal by the CVD method. The modified surfaces exhibit superhydrophobicity (WCA > 160°) and low hysteresis (<1°). These superhydrophobic coatings demonstrated resistance to acid, alkali, and salt solutions. Compared to bare copper, the superhydrophobic coating significantly improved corrosion protection by three orders of magnitude.

Chang *et al.*[127] replicated the surface structure of fresh leaves of Xanthosoma sagittifolium using PDMS. They then obtained a superhydrophobic epoxy/organophilic clay (SEC) coating on cold-rolled steel through a 3D-bioprinting technique. The SEC obtained by this biomimetic technique effectively prevented corrosion of the metal substrate by O_2, H_2O, and aggressive ions. Similarly, Chang *et al.*[128] prepared a hydrophobic epoxy/graphene composite coating using a nanocomposite casting method and simulated the leaf structure (Xanthosoma sagittifolium leaves) using a PDMS polymer template. The resulting hydrophobic surface provided higher corrosion resistance than uncoated rolled steel. Crosslinked polybenzoxazine (PBZ)-based coatings prepared by Zachariah *et al.*[129] using lotus leaf and xanthosoma sagittifolium leaves as templates had a hierarchical surface structure and high hydrophobicity. The coating showed 99.93% protection efficiency compared to the corrosion rate of the normal PBZ coating. The biomimetic concept of introducing a hierarchical surface structure and hydrophobicity on the surface of anticorrosive coatings has a significant effect on improving corrosion protection efficiency.

Vicente *et al.*[130] deposited poly(acrylic acid) + β-cyclodextrin (PAA + β-CD) onto an aluminum alloy substrate using electrostatic spinning. They then obtained a PTFE layer by simple spin-coating, and finally, a layer of PTFE particles was electrosprayed to provide high roughness, resulting in a superhydrophobic coating with a hydrophobicity angle greater than 170°. The Cassie state created by this method greatly reduced the contact area between the coating and the liquid, acting as an effective barrier against the penetration of corrosive media into the underlying metallic substrate. As a result, the corrosion rate was reduced by four orders of magnitude. The technique with the preparation of superhydrophobic surfaces is presented in Fig. 9.

3.4. Biomimetic superhydrophobic surface applications

3.4.1. Superhydrophobic self-cleaning anti-corrosion surfaces. Self-cleaning surfaces inherently possess the capacity to eliminate dirt particles effortlessly. Specifically, superhydrophobic surfaces exhibit self-cleaning attributes by efficiently repelling water molecules, enabling water to smoothly roll over the surface and facilitate the removal of dirt. Conversely, the self-cleaning mechanism of hydrophilic surfaces operates through diffusion. In this process, water on the surface diffuses, effectively carrying away dirt particles from the solid surface. The widespread application and advancement of self-cleaning technology trace their origins to the innate superhydrophobic characteristics of lotus leaf surfaces.[21]

In a study reported by Li *et al.*[131] superamphiphilic CuO films with exceptional self-cleaning and corrosion resistance were prepared on the surface of the steel, which was achieved through a combination of electrodeposition, solution immersion, and fluoride modification. The multilevel structure, comprising micro-floral structures and secondary nanosheets, demonstrated the ability to repel both water and glycerol. The authors utilized fly ash with a particle size of tens of micrometers to dedust the superamphiphobic CuO film, with contaminants easily removed by 8 μL water droplets. Shu *et al.*[132] employed nanosecond laser processing technology and the sol–gel method to design and fabricate mechanically robust micro- and nanostructures. They developed modified SiO_2@PDMS superhydrophobic corrosion-

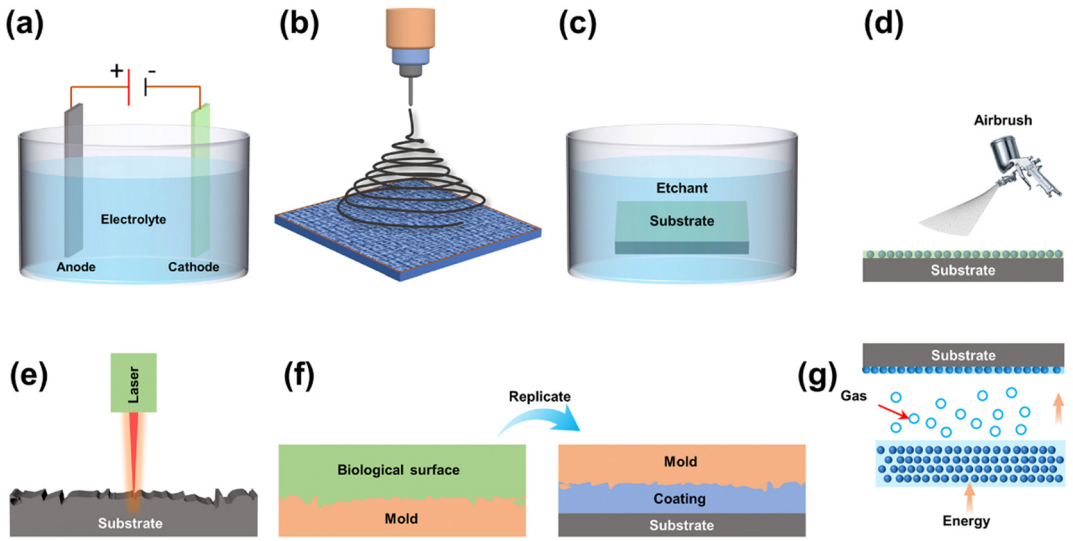

Fig. 9 Schematic representation of a common manufacturing method for bio-inspired microtextured surfaces, including (a) electroplating, (b) electrospinning, (c) chemical etching, (d) spray coating, (e) laser processing, (f) template method, and (g) CVD.

resistant coatings on copper substrates. The authors utilized micron-sized fly ash particles as contaminants and relied on the ultra-low water adhesion (3.27 μN) on the surface to automatically remove dust within 200 s. Even after sandpaper abrasion, tape peeling, and cross-scratch tests, the coating maintained good superhydrophobicity. Jiang *et al.*[133] prepared a ZnO@ZIF-8 superhydrophobic anti-corrosion coating on a magnesium alloy substrate, which involved micro-arc oxidation coating as a transition layer, followed by ZnO nanorods as a sacrificial template and Zn^{2+}-induced growth of ZIF-8 on the surface through ligand solution etching. The corrosion resistance of the ZnO@ZIF-8 superhydrophobic coating significantly improved compared to that of untreated AZ91D. Chalk dust was used as a contaminant, and the study demonstrated that water droplets could easily carry away contaminants on the surface by tilting it at a certain angle.

3.4.2. Superhydrophobic anti-fouling anti-corrosion surfaces. The marine environment serves as a highly corrosive electrolytic cell, where continual chemical and electrochemical reactions occur with the metal substrate. Furthermore, electrochemical corrosion results in the formation of material voids and gaps, creating favorable conditions for microbial adsorption and reproduction, thereby exacerbating biological corrosion. In scenarios such as sea-traveling cargo ships and submarines submerged in seawater, the adhesion of microorganisms leads to reduced navigation speed and increased fuel consumption. Undesirable adsorption and accumulation of microorganisms, algae, and organic matter in seawater contribute to the formation of biofouling—a gradual process encompassing four stages.[134] In the initial stage, organic molecules and inorganic particles are adsorbed to the material surface, forming a base film within seconds or minutes through physical and electrostatic adsorption. Subsequently, algae in seawater attach to the base film within hours, constituting a reversible attachment. The third stage involves the growth and multiplication of bacteria over a few days, attracting other microorganisms and algae to form microfouling. In the fourth stage, organisms like barnacles and mussels attach to the microfouling biofilm within weeks, leading to the development of macrofouling. Microbial adhesion in complex environments accelerates material dissolution and metal oxidation, potentially resulting in holes and cracks formed by biofouling. Nature has developed various protective mechanisms against marine biofouling over evolutionary periods. One such mechanism involves the creation of an air cushion layer on the surface, mimicking the bionic superhydrophobic nature, which effectively blocks corrosive marine media such as Cl^-. Importantly, superhydrophobic surfaces prevent the formation of a base film from the initial stage and exhibit superior repellent properties against biofouling adhesion.

Philip *et al.*[135] reported the fabrication of superhydrophobic titanium surfaces using simultaneous anodic oxidation and adsorption with an ethanol solution of myristic acid and HCl. Exposure of these surfaces to microbial cultures for 48 hours resulted in a 50% reduction in bacterial adhesion compared to bare surfaces. Rasitha *et al.*[136] developed robust SHSs by covalently bonding hydrolyzed glycidoxypropyltrimethoxysilane to a hydrophilic aluminum substrate as an intermediate layer, with hexamethyldisilazane-modified nano-silica as the top low surface energy material. The surface exhibited good self-cleaning ability, and the corrosion current density was significantly reduced compared to bare samples. Selim *et al.*[137] synthesized silicone/GO-Fe_3O_4 nanocomposites inspired by composite mosquito eyes and dispersed into PDMS to obtain coatings with superhydrophobic properties showing high anti-fouling efficiency. The homogeneous dispersion of GO-Fe_3O_4 nanofillers had a good growth inhibition effect on microorganisms (Kocuria rhizophila, *Pseudomonas aeruginosa*, and Candida albicans) with good growth inhibition. Surface roughness and superhydrophobicity enhanced the antifouling adhesion and significantly reduced the number of adherent bacteria.

In a parallel approach, inspired by the multifaceted ability of kelp to inhibit marine pollution through a combination of physical micromorphology, chemical composition, and bioactive substances, Zhao *et al.*[138] incorporated capsaicin into nanocapsules. These nanocapsules were stably deposited on modified PDMS surfaces, resulting in the development of novel PDMS antifouling coatings with multiple synergistic antifouling properties, utilizing the LBL assembly method. The microstructured surface of the biomimetic antifouling material played a crucial role in reducing the attachment points of fouling organisms, while the highly hydrated polymer film on the surface contributed to the reduction in algae adhesion. Moreover, the introduced nanocapsules demonstrated an additional enhancement of antifouling performance by leveraging bacteria as a stimulation switch, controlling the release rate of bioactives within the coatings.

3.5. Challenges and strategies for superhydrophobic anti-corrosive surfaces

As previously mentioned, biomimetic superhydrophobic surfaces have demonstrated significant self-cleaning, anti-pollution, and anti-corrosion effects, hinging on the maintenance of a stable liquid–air interface on the surface, earlier referred to as the Cassie state. However, several factors, including mechanical friction, chemical stability, and a gradual decline in air pressure within the confined cavity due to an elevation in liquid pressure, render the surface susceptible to transitioning from the Cassie state to the Wenzel state or even experiencing a complete loss of water resistance. The precarious stability of superhydrophobic surfaces poses a substantial challenge, acting as a hindrance to the advancement of their applications. Consequently, the construction of interface-strengthened superhydrophobic surfaces has emerged as a focal point of research in recent years.

3.5.1. Mechanical durability. Superhydrophobic surfaces with high contact angles and low rolling angles can be obtained by introducing nano- or micrometer-scale morphologies. However, the stability of such structures is challenged as mechanical instability leads to a loss of robustness. Wang *et al.*[139] used the concept of armored structures to improve mechanical stability and synthetic techniques for coatings on substrates to provide superior strength (Fig. 10). Using binders is considered to be an effective method to improve the robustness of

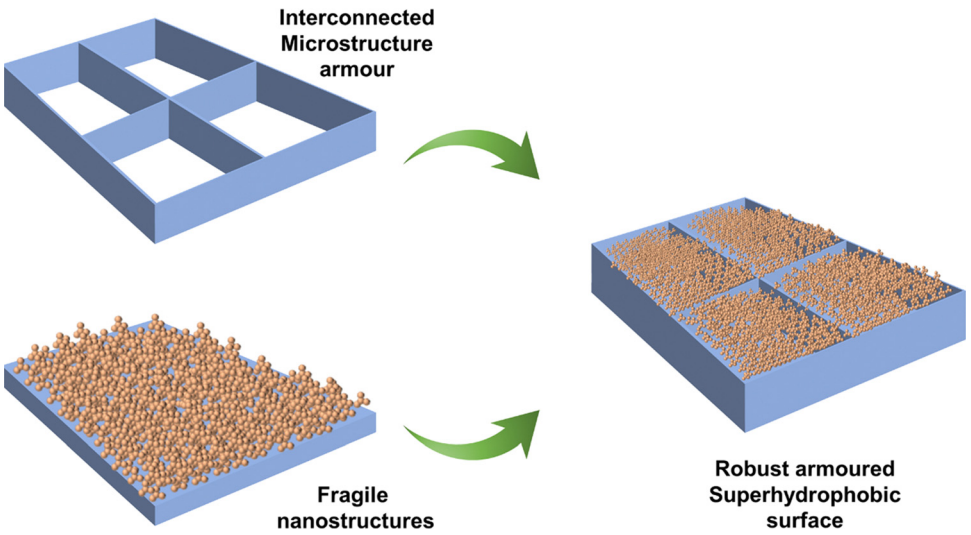

Fig. 10 Design concept of the robust armoured superhydrophobic surface.

SHSs. Typically, a binder is used to strengthen the interface between a substrate and a hydrophobic material, and hydrophobic particles are added to build up the rough structure. Specifically, there are several combinations of this technique, including mixing the adhesive and hydrophobic particles, using the adhesive as an intermediate layer and the hydrophobic particles as a surface layer, and mixing the adhesive and hydrophobic particles. Of these, the first two combinations are more common. For example, Chen *et al.*[140] prepared hydrophilic nano-ZIF-8 with hydroxyl groups using MOF (ZIF-8) nanoparticles and organic resins as a substrate at room temperature and then hydrolytically condensed nano-ZIF-8 modified with low-surface-energy perfluoroalkyltriethoxysilanes (POTS) to produce SHSs.The coating was improved by introducing epoxy resin (EP) as an adhesive layer to improve its robustness and adhesion. The prepared ZIF-8/POTS/EP composite coatings exhibited good water repellency and mechanical and chemical stability and remained superhydrophobic after 300 days of aging in air or 60 days of immersion in 3.5 wt% NaCl aqueous solution. In addition, Zhang *et al.*[141] successfully prepared purely hydrophobic PDMS surfaces and superhydrophobic candle soot (CS) deposited surfaces, as well as bilayer PDMS-CS coatings by scraping and CS incomplete combustion deposition. PDMS acted as a binder in the composite coatings, effectively connecting the outer layer of CS to the bottom aluminum substrate. The cohesive properties of PDMS, the nano-structures of the porous network, and the very low surface energy of the deposition due to incomplete combustion of candles together contribute to the formation of a corrosion-resistant and robust coating.

In addition to incorporating binders, the creation of durable SHSs can be achieved through the construction of ordered structures. These structures can generate micro/nanometer-scale deformations that exhibit cross-scale characteristics and are highly correlated with wear strength. Zhang *et al.*[142] employed a one-step hydrothermal method to manufacture hierarchical micro/nanostructured superhydrophobic ZnO/Cu-ZnMOFs@SA composite coatings, exhibiting enhanced corrosion protection. This enhancement is attributed to both the hierarchical micro/nano-structures and the stearic acid (SA) modification, which collectively hinder aggressive ion transport. The hierarchical micro/nano-structure of ZnO/Cu-ZnMOFs@SA ensured that the surface retained its roughness even after rubbing, and delamination was visibly mitigated. Notably, the superhydrophobic properties could be easily restored by re-immersion in an ethanol solution containing SA.

3.5.2. Deep water pressure. Apart from mechanical stability, one of the primary challenges encountered by SHSs during underwater use is the infiltration of water within air pockets due to the influence of high liquid pressures, leading to their instability. In underwater environments, such as submarine equipment exposed to seawater conditions, the coating surface experiences submergence under varying hydrostatic pressures at different depths. The disruption of air pockets on the superhydrophobic coating surface adversely affects the protective capability of the coating.[143] Poetes *et al.*[144] investigated the stability of underwater superhydrophobic surfaces and found that the air layer enclosed in the microstructure readily diffuses into the water, thus altering the surface wettability. Manoj *et al.*[145] investigated the effect of water pressure on the wetting and corrosion behavior of superhydrophobic coatings. Under high hydrostatic pressure, the coating absorbs a large amount of water into the voids, which ultimately leads to the loss of superhydrophobicity and corrosion resistance. Typically, once a superhydrophobic surface is fabricated, it is not possible to adjust the solid–liquid contact area to the dynamic environment. Recently, smart surfaces with different air cushion ratios have been demonstrated, either using soft materials or multilayer structures in response to external stimuli.[146–148] A better solution may be to develop superhydrophobic surfaces with adaptive morphology to the forces exerted by the liquid (*i.e.*, liquid pressure) to regulate the solid–liquid stability in the face

of dynamic environments. Tan *et al.*[149] proposed a bilayer-structural liquid-pressure-guided superhydrophobic surface (LPGSS) consisting of a rigid micropillar array and a soft PDMS on top (Fig. 11). The results show that the LPGSS can maintain a stable Cassie state during droplet compression. The LPGSS can effectively adapt itself to the radius of the PDMS in response to changes in liquid pressure and protect the air cushion from damage. However, the mechanical durability of the soft surface still needs to be considered. Therefore, studying and improving the stability and durability of SHSs remains a key research direction to make it a reliable and long-lasting anti-corrosion technology.

3.5.3. Self-healing superhydrophobic surfaces. Most SHSs are susceptible to scratches and abrasions during use, resulting in the degradation of their structures. Additionally, the low-surface-energy substances modified on these surfaces are susceptible to decomposition caused by factors such as light radiation, exposure to organic pollutants, and strong acids and bases. This decomposition leads to the loss of superhydrophobicity, significantly diminishing the service life of superhydrophobic surfaces and constraining their widespread adoption in practical applications. As discussed in Section 3.5.1, researchers have sought to enhance mechanical durability by incorporating adhesives into the fabrication of superhydrophobic surfaces. However, these surfaces are essentially "disposable" and cannot regain their original superhydrophobic properties after sustaining damage. To address this limitation, the integration of self-repairing features into superhydrophobic surfaces, making them self-healing, emerges as a promising strategy to extend their service life. Inspired by the natural regenerative abilities of damaged clover, where the rough structure and chemical composition can be regenerated, researchers have combined self-healing capabilities with superhydrophobicity to create self-healing superhydrophobic surfaces. These surfaces can be recycled, presenting an innovative approach for achieving the long-term durability of artificial superhydrophobic surfaces. Typically, the preparation of self-healing superhydrophobic surfaces involves inducing the migration of low surface energy substances or the reconstruction of rough structures.

Chemical or mechanical stimuli from within the coating or underlying low surface energy materials can drive the disrupted low surface energy materials to migrate to the surface in cases where the microstructures of SHSs remain intact or experience limited disruption. This migration helps in regaining the superhydrophobicity of the surface.[150–152] Wang *et al.*[153] conducted a simulation of the structure found on lotus leaves and employed a template method to fabricate a self-healing superhydrophobic PDMS/*n*-nonadecane wax composite surface. By replicating the nipple structure, the surface achieved the desired roughness, and the incorporation of *n*-nonadecane wax provided a low surface energy, imparting superhydrophobicity to the surface. Following an oxygen plasma treatment, the surface became rich in hydroxyl groups, undergoing a transition from superhydrophobic to superhydrophilic. Intriguingly, after 20 minutes of storage at room temperature, the surface was able to regain its superhydrophobicity. Fig. 12 illustrates the fundamental process of this self-healing behavior. The difference in interfacial free energy drives the transport of hydrophobic waxes from the PDMS matrix to the surface, reducing the surface energy and restoring rough fibers on the microscale structure. The high mobility of the PDMS molecular chains further facilitates the diffusion of *n*-nonadecane molecules within the PDMS network. The combined effect of these factors results in rapid transport kinetics of hydrophobic wax molecules from the physical structure to the outer surface, facilitating the repair of superhydrophobicity. Additionally, low

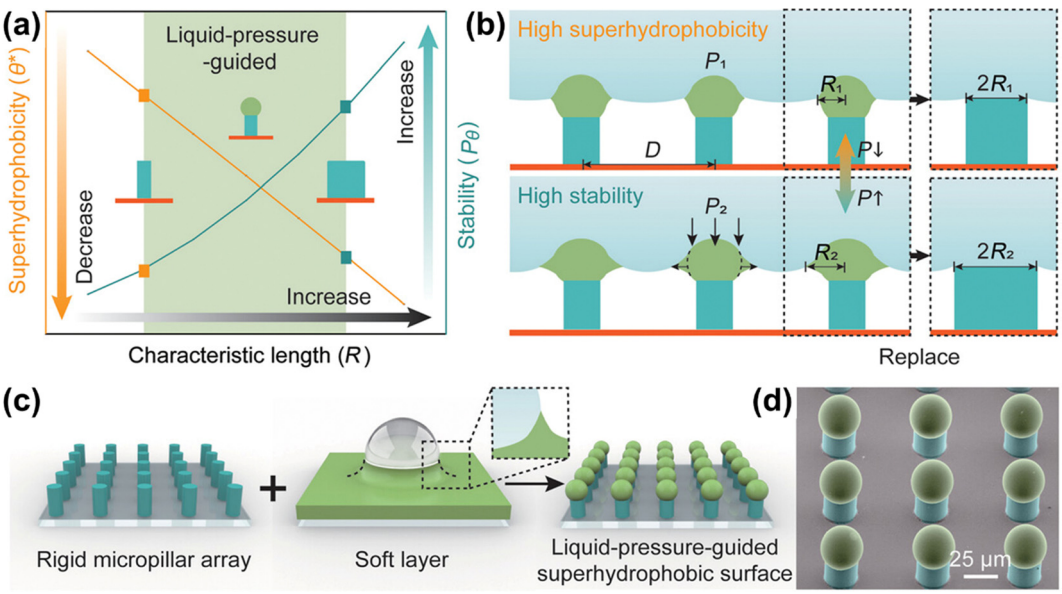

Fig. 11 Design of a bilayer-structural liquid-pressure-guided superhydrophobic surface (reproduced from ref. 149 with permission from [Wiley], copyright [2022]).

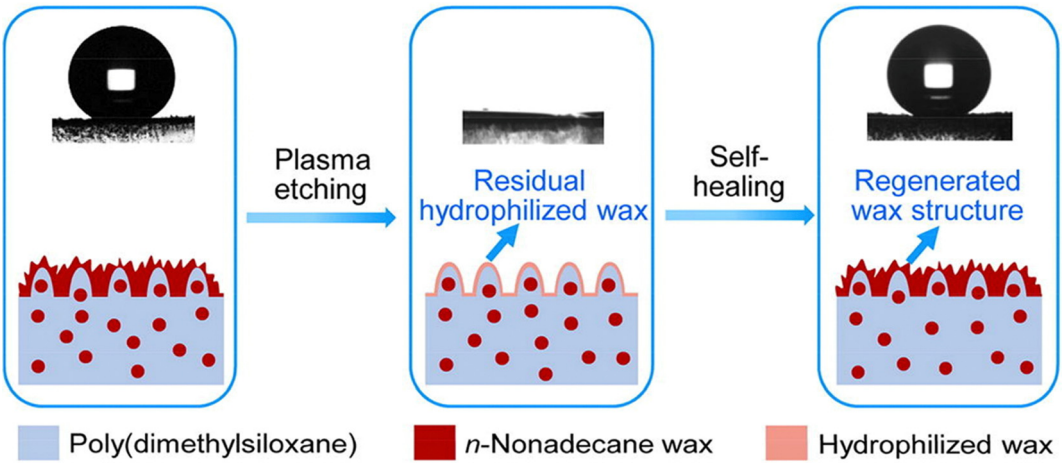

Fig. 12 Schematic representation of the self-healing mechanism of SHSs (reproduced from ref. 153 with permission from [Elsevier], copyright [2020]).

surface energy substances can be stored in microcapsules in advance. In the event of chemical damage to the surface, the low surface energy substance is released from the container under external stimuli, migrating to the surface and thereby achieving the recovery of superhydrophobicity. Uzoma *et al.*[154] utilized polymerization to synthesize microcapsules containing fluorosilane and urea-formaldehyde as core-shells. These microcapsules were incorporated into fluorocarbon resins and sprayed onto aluminum alloy substrates to develop self-healing superhydrophobic coatings. Following oxygen plasma treatment or alkali treatment, the coating initially lost its superhydrophobicity. However, after 8 days at room temperature, the coating managed to regain its initial superhydrophobicity due to the gradual release and migration of fluorosilane from the microcapsules to the coating surface. EIS results indicated that the released hydrophobic fluorosilane performed well in corrosion inhibition.

The migration of low surface energy materials is typically suitable for repairing superhydrophobic surfaces under specific conditions such as plasma etching, chemical damage, and slight wear. However, in practical usage, superhydrophobic surfaces are more likely to face damage to their rough structures. In such cases, achieving the repair of superhydrophobic properties solely through the migration of low surface energy substances becomes challenging. Compared to the self-healing of low surface energy materials, the self-healing of surface-grade rough structures is more intricate, particularly when dealing with large-scale structural damage. To address this challenge, structural regeneration through rearranging components and polymers in the coating can effectively repair damage at the nano-scale or even micrometer scale.[155–157] Wang *et al.*[158] synthesized ACNTB-SiO_2-KH570 particles by combining KH570-modified nano SiO_2 with oriented carbon nanotube bundles (ACNTBs). These particles were used to prepare EP/ACNTB-SiO_2-KH570 composite superhydrophobic surfaces together with EP. The particles provided the necessary hierarchical structure, ensuring the ideal mechanical stability of the surface. When the EP/ACNTB-SiO_2-KH570 surface was damaged and removed with tape, the water contact angle decreased to 123°. Interestingly, after heating the damaged surface at 300 °C for 9 hours, the contact angle rebounded to 160°, and the water resistance remained stable after multiple cycles of structural damage and regeneration. The schematic self-healing mechanisms mediated by structural regeneration are illustrated in Fig. 13(a). During heating, the EP polymer partially breaks down, exposing layered nanoparticles. The heat energy weakens the interaction between ACNTB and SiO_2. Gases generated from the EP polymer decomposition further accelerate the transport and assembly of SiO_2 nanoparticles to reconstruct the rough structure on the damaged surface, facilitating the self-healing process triggered by structural regeneration.

Another approach to achieving the regeneration of shape relies on SMP. SMP is a stimulation-responsive material that can be restored from a temporarily deformed shape to its original form through external stimuli. Utilizing SMP for the preparation of superhydrophobic surfaces allows for the complete repair of deformed structures.[159,160] Zhang *et al.*[161] scraped SMP emulsion containing ceresine wax microparticles and BTA onto the surface of the magnesium alloy matrix and then sprayed fluorinated attapulgite (fluorine ATP) suspension to obtain SHSs (Fig. 13(d)). SMP is self-healing based on the shape memory effect, which can repair locally damaged areas. However, the formation of corrosion products prevents the closing of physical scratches, making it difficult for SMP coatings to recover their initial anti-corrosion properties. The introduction of BTA delays the occurrence of corrosion to a certain extent, so even if the SMP-BTA coating is not repaired in time, the coating can still partially recover its anti-corrosion properties. The top layer of fluorine ATP can effectively prevent corrosive electrolyte penetration into the coating by maintaining an air cushion at the solid–liquid interface. Therefore, the synergistic effect of SMP-BTA and the fluorine ATP layer results in the coating being almost completely self-healing, thus restoring the corrosion resistance.

The compensation of low surface energy materials and the reconstruction of rough structures enable the self-healing of

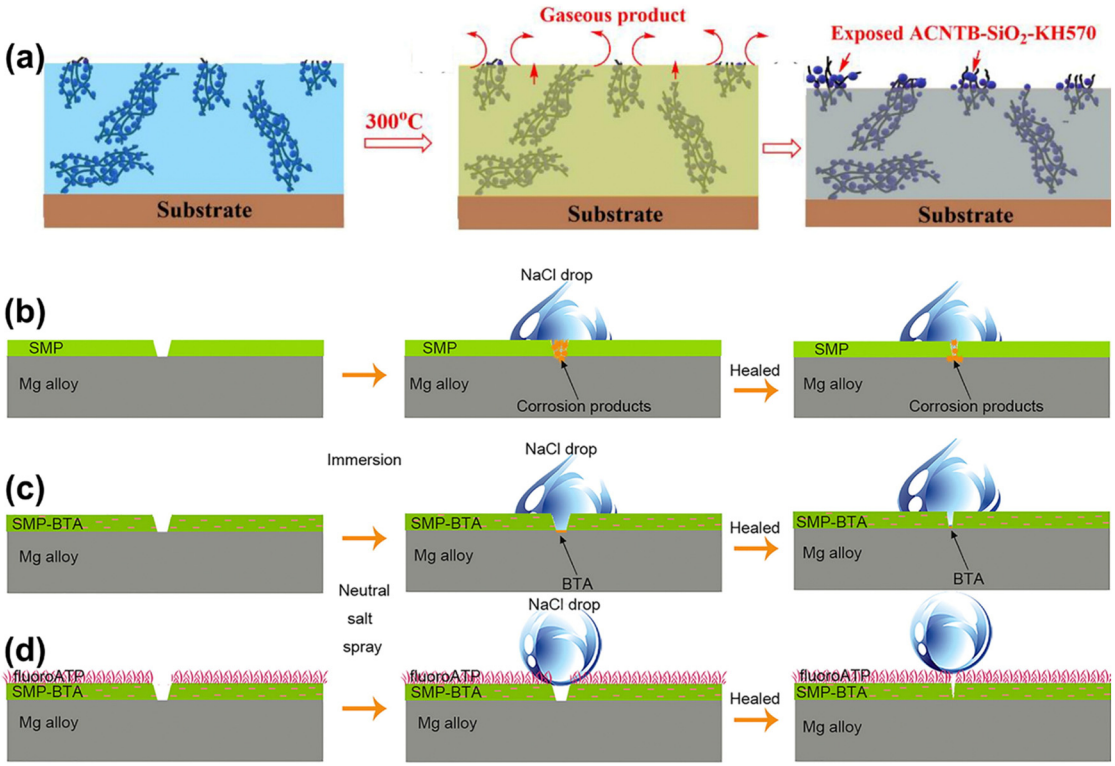

Fig. 13 (a) Schematic of the self-healing mechanism of EP/ACNTB-SiO_2-KH 570 of the damaged coating (reproduced from ref. 158 with permission from [Elsevier], copyright [2020]). Self-healing mechanism of the (b) SMP, (c) SMP-BTA, and (d) SMP-BTA/fluoroATP coatings (reproduced from ref. 161 with permission from [Elsevier], copyright [2021]).

superhydrophobic properties. However, many self-healing SHSs often require elevated temperature, light, or other external stimuli to expedite the repair process, making it challenging to achieve rapid repair at room temperature. Moreover, there has been relatively limited research on millimeter-scale or even centimeter-scale damage. Future development in this field is anticipated to focus on optimizing the design of coating structures and self-healing conditions. The aim is to develop superhydrophobic coatings that can efficiently and quickly self-repair large-size damage at room temperature. This optimization will be crucial for expanding the practical applications of self-healing superhydrophobic surfaces.

4. Biomimetic slippery liquid-infused porous surface

The bottle-shaped insect trap of Nepenthes features an inner wall with a porous microstructure and is filled with lubricating fluid. This unique attribute effectively prevents insects from escaping by leveraging the super-slip property of the inner wall. Fig. 14(a). Bohn *et al.*[162] discovered that the inner wall's special microstructure securely traps the waxy mucus secreted by the inner wall, forming a continuous liquid surface within the cage. In 2011, Wong *et al.*[163] pioneered the synthesis of slippery liquid-infused porous surfaces (SLIPSs), drawing inspiration from Nepenthes. SLIPSs utilize micro-textures to immobilize the lubricant on the substrate, serving as a repellent. By injecting the lubricant into the micro/nano-structures, a continuous and uniform dynamic liquid layer forms on the substrate's surface, effectively shielding the metal from corrosive media. The researchers conducted a comparison between the electrochemical impedance spectra and polarization curves of SLIPSs and SHSs. The results showed that the electrochemical impedance of SLIPSs is typically 2–3 orders of magnitude higher than that of SHSs, and the corrosion current density is 1–2 orders of magnitude lower than that of SHSs. Furthermore, the electrochemical impedance values of SHSs decreased more rapidly during long-term immersion in corrosive media, whereas SLIPSs demonstrated superior long-term corrosion resistance.[164–168]

4.1. Challenges and strategies for SLIPSs

In contrast to the preparation of SHSs, where SLIPSs need to align matrix material properties with lubricant properties, chemical coatings can be applied to enhance material-lubricant affinity. Two common methods for inducing low-energy chemical coatings involve liquid phase deposition through a dip coating or spraying techniques in the first and the use of CVD to functionalize the surface in the second.

Wong *et al.*[163] proposed three essential requirements for the thermodynamic stability of SLIPSs. First, the lubricant must quickly inhale, moisten, and stably attach to the substrate surface to prevent test fluid penetration and displacement of the lubricant. Second, the solid surface should be preferentially

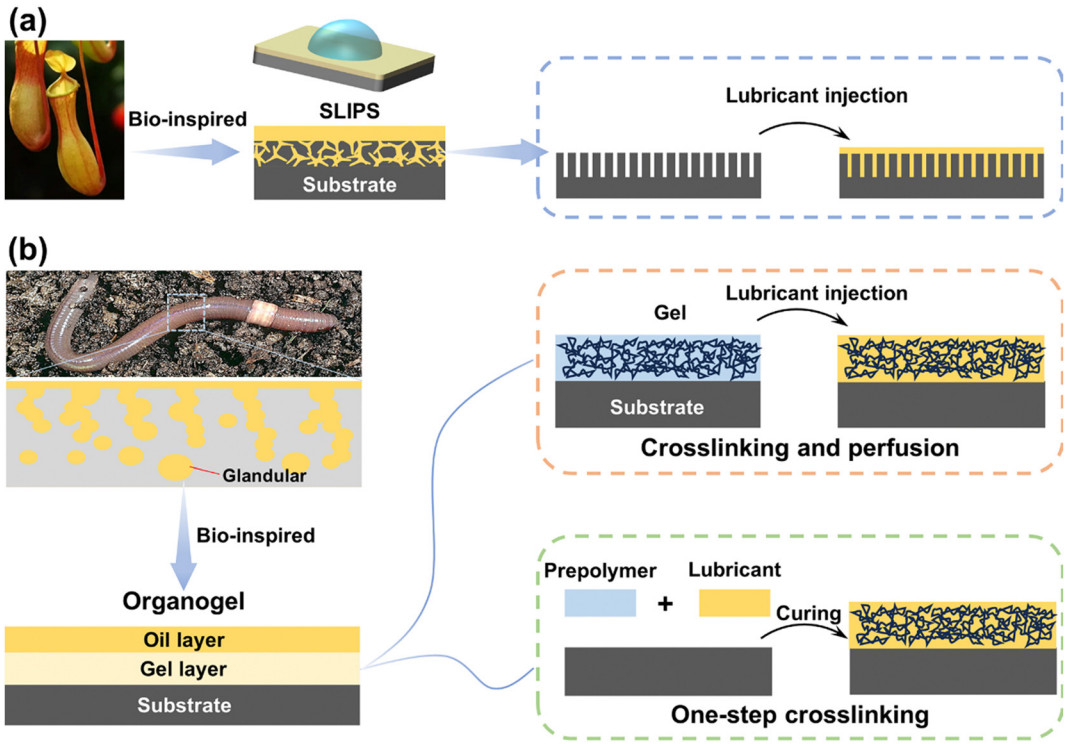

Fig. 14 Schematic representation of the bio-inspired surfaces: (a) SLIPSs and (b) organogels and their preparation methods.

wet with the lubricant rather than the liquid to be repelled. Third, the lubricant and impact test fluid must be incompatible. Deterioration mainly stems from lubricant depletion and porous layer destruction, highlighting the importance of the matrix morphology and lubricant in designing SLIPSs with excellent sliding properties.

The size and nature of substrate holes are critical for strong lubricant anchoring. Suitable roughness enhances stable lubricant retention through capillary action and van der Waals forces. Small pore sizes and high porosity in substrates contribute to durability by generating high capillary pressure to retain the lubricant and allowing a larger contact area for effective self-cleaning. The creation of micro/nanostructures with roughness on SLIPSs substrates mirrors techniques used for SHSs, as described in Section 3.3.

The design and preparation of SLIPSs should center on selecting lubricants with properties suitable for the service environment. Table 3 outlines commonly used lubricants for anticorrosion SLIPSs. Additionally, extensive research has delved into the viscosity–durability relationship of SLIPSs.[169–172] Findings reveal that higher viscosity lubricants facilitate droplet retention with superior durability, while low viscosity lubricants excel in sliding properties.

Despite diligent research efforts made to enhance lubricant retention, depletion of lubricants remains an unavoidable occurrence across multiple application cycles. Drawing inspiration from the constant secretion of mucus by biological sebaceous glands to lubricate and moisturize the skin, solid materials with three-dimensional cross-linked networks that serve as reservoirs for lubricants are denoted as organogels, offering an alternative to SLIPSs. The synthesis of organogels can be achieved through two distinct approaches, as shown in Fig. 14(b). Firstly, by dissolving a well-cured polymer network, organogels are formed, where the lubricant interacts with the network structure, balancing the entropy and enthalpy of polymer chain mixing, thereby immobilizing the lubricant and giving rise to the organogel. Alternatively, the incorporation of the lubricant into the cured prepolymer results in the storage of the lubricant within the polymer network structure, leading to organogel formation.[181–184] Organogels present several advantages, including tunability, dynamic self-healing capabilities, and facile synthesis. Nevertheless, the presence of the lubricant in the organogel diminishes its affinity with the metal substrate, predisposing the system to corrosion at the coating-metal interface. Consequently, enhancing the bond between the substrate and the organogel emerges as a crucial research direction.

4.2. Anticorrosion mechanism on SLIPSs

The lubricating liquid injected into the micro-nano structure of SLIPSs forms a continuous dynamic liquid film on the substrate surface. This film hinders direct contact between the substrate surface and the corrosive medium, preventing the transfer of electrons from the anode to the cathode and enhancing the corrosion resistance of the metal. Simultaneously, the low adhesion characteristics of the liquid film prevent direct contact between microorganisms and the matrix, effectively inhibiting microorganism adhesion and preventing microbial corrosion (Fig. 15(a)).[185–188] In the organogel, the silicone oil layer on the surface acts as a barrier during the

Table 3 Commonly used lubricants of SLIPSs for anti-corrosion

Type	Substrate	I_{corr} (A cm^{-2})	E_{corr} (V)	R_{ct} (Ω cm^2)	Ref.
Silicone oil (DC-200)	AZ31B Mg alloy	1.918×10^{-6}	−1.331	—	164
Silicone oil (200 mPa s)	1060 Al alloy	1.85×10^{-10}	3.17	—	173
Silicone oil (20 mPa s)	AZ31 Mg alloy	1.17×10^{-9}	—	1.34×10^{7}	174
Silicone oil (10 mPa s)	Al plates	5.0×10^{-12}	−0.35	1×10^{7}	175
Krytox 104	Al foil	—	−0.651	—	176
Krytox GPL 103	AZ31 Mg alloy	3.44×10^{-10}	−0.210	55.9×10^{6}	177
Krytox 100	Mild steel	3.687×10^{-8}	−0.338	1.80×10^{6}	178
Plant oil	Q235 steel	—	—	1.42×10^{10}	179
Ionic liquids	Al alloy	7.8×10^{-9}	0.712	—	180

initial impregnation of the corrosion system, preventing the penetration of external water molecules into the coating. When the thin silicone oil layer is destroyed, water molecules reach the substrate surface through some unfilled voids, leading to local corrosion. However, the majority of the gel voids are still filled with silicone oil, inhibiting the diffusion of the corrosive medium (Fig. 15(b)).[189]

4.3. Application of SLIPSs in anticorrosion

4.3.1. Steel alloys. Steel and its alloys stand as crucial engineering materials widely employed in daily life and various industrial fields.[190] However, when exposed to aggressive ions, such as halogen ions, steel is susceptible to passivation film breakdown and pitting corrosion.[191] Corrosion-induced structural failures and safety incidents are common, particularly for steel engineering structures operating in corrosive environments. The service life of these structures predominantly relies on the effectiveness of corrosion protection. Consequently, enhancing the stability of alloy steels in corrosive environments is a significant challenge. The investigation of SLIPSs holds great importance in enhancing the corrosion resistance of steel and broadening its application scope. Various methods are employed for preparing SLIPSs on steel, including electrodeposition, anodic oxidation, and spraying.

Xiang *et al.*[192] utilized the electrodeposition method to create a coating with a porous metal film using a hydrogen bubble template. They injected a PDMS/paraffin mixture after FAS modification, forming a slippery surface composed of three solid layers (Fig. 16). This coating exhibits good corrosion resistance, with a corrosion current density of 6.402×10^{-9} A cm^{-2} and an impedance of 2.301×10^{7} Ω cm^{-2}, two orders of magnitude higher than those of the pure Ni coating. Additionally, Bae *et al.*[193] employed anodization to generate a nano-porous oxide layer with microscopic roughness on the surface of stainless steel, providing storage conditions for lubrication. They coated the nano-porous oxide layer with a stearic acid solution without fluorine, transforming it into a hydrophobic surface. Finally, they impregnated the nano-porous oxide layer with edible oil to achieve corrosion resistance, environmental protection, and anti-condensation. Zhang *et al.*[194] prepared a coral clustering structure SiO_2 coating on carbon steel surfaces using a spraying

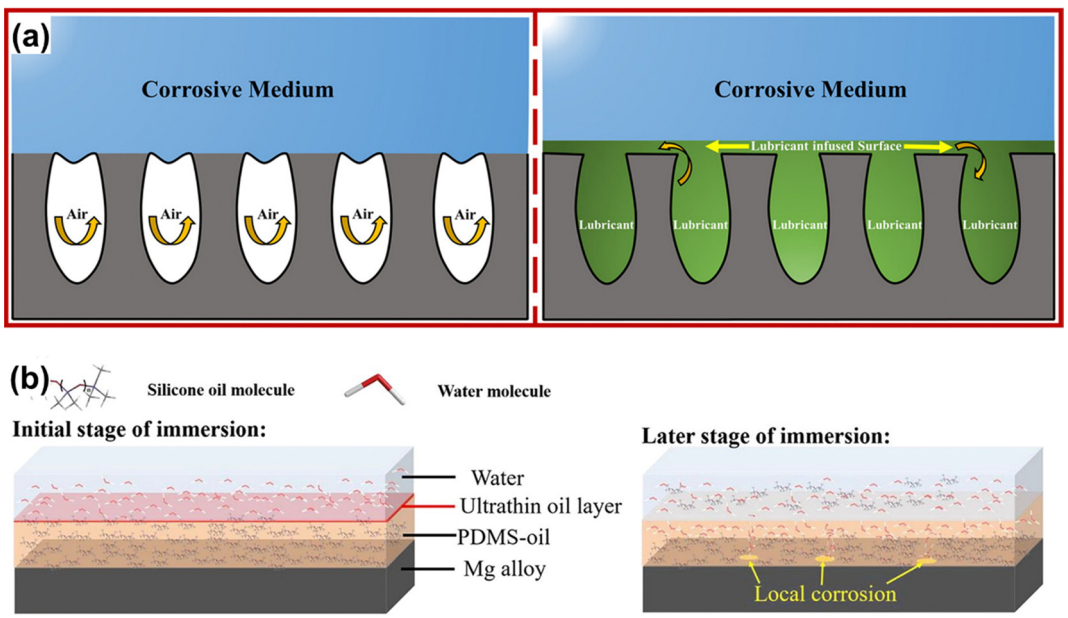

Fig. 15 Corrosion prevention mechanism of (a) SHSs and SLIPSs (reproduced from ref. 188 with permission from [Wiley], copyright [2021]) and (b) organogel (reproduced from ref. 189 with permission from [Elsevier], copyright [2021]).

method. The coating exhibited excellent silicone locking ability, as confirmed by the EIS results demonstrating outstanding corrosion resistance.

4.3.2. Titanium alloys. Titanium alloys are recognized as the "marine metal" in the marine field due to their outstanding anti-corrosion properties and comprehensive mechanical characteristics.[195] Despite their excellent corrosion resistance, titanium alloys may experience corrosion under specific conditions such as exposure to acid, alkali, salt solutions, and high temperatures. These environmental factors can induce chemical reactions in titanium alloys, leading to damage to their surface and internal structure.[196] Additionally, titanium alloys, known for their good biocompatibility, are more susceptible to serious biological pollution in the marine environment compared to other structural materials, posing a significant threat to their long-term safety and function. Historically, paints containing toxic heavy metal ions were commonly used to repel or eliminate organisms attached to titanium alloy surfaces, a practice at odds with the growing global consensus on environmental protection.[197] In the quest to enhance the corrosion resistance and biological adhesion resistance of titanium alloys, researchers are exploring new effective methods. Among these, slippery surface technology is considered to have significant application potential in the field of titanium alloy corrosion prevention.

Yue *et al.*[198] employed micro-arc oxidation technology and chemical modification to *in situ* prepare SLIPSs on the surface of titanium alloys (Fig. 17(a)–(c)). SLIPSs comprise micro/nanopores produced by micro-arc oxidation, providing lubricant storage, and nano-skin spikes produced by the hydrothermal method that firmly retains the lubricant. Experimental results reveal that the coverage of chlorella and Phaeodactina trichotriangle on SLIPSs is 2 to 3 orders of magnitude lower than that on traditional titanium alloy surfaces, indicating that the new synovial material exhibits remarkable stability, durability, biological contamination resistance, and corrosion resistance. Wang *et al.*[199] utilized anodic oxidation to grow *in situ* nanostructures with different diameters and depths, including nanopores and nanotubes, on the surface of titanium alloys (Fig. 17(d)–(g)). Fluorosilane is used to reduce the surface energy, ensuring easy immersion of the lubricant into the nano-structure. Owing to the super-slippery properties of the lubricant layer, this coating demonstrates significant stain resistance against *E. coli* and Navicula exigua. Simultaneously, SLIPSs improve the corrosion resistance of titanium alloys and play a synergistic role as the anode film, carburizing layer, and lubricant layer.

4.3.3. Copper alloys. Copper-based materials, renowned for their impressive mechanical properties and thermal conductivity, find widespread use across various industries. However, these materials encounter challenges in the form of environmental corrosion, especially when exposed to elements like seawater, acidity, and alkalinity.[200,201] Shi *et al.*[202] addressed this by oxidizing copper foil with copper chloride, sodium hydroxide, sulfuric acid, and other reagents to form nano-scale needle-like copper hydroxide on its surface. Subsequently, they modified it with an ethanol solution mixed with dodecyl mercaptan and injected a perfluorinated lubricant to achieve a super-smooth surface. The use of a Scanning Kelvin probe demonstrated an increase in electric potential from

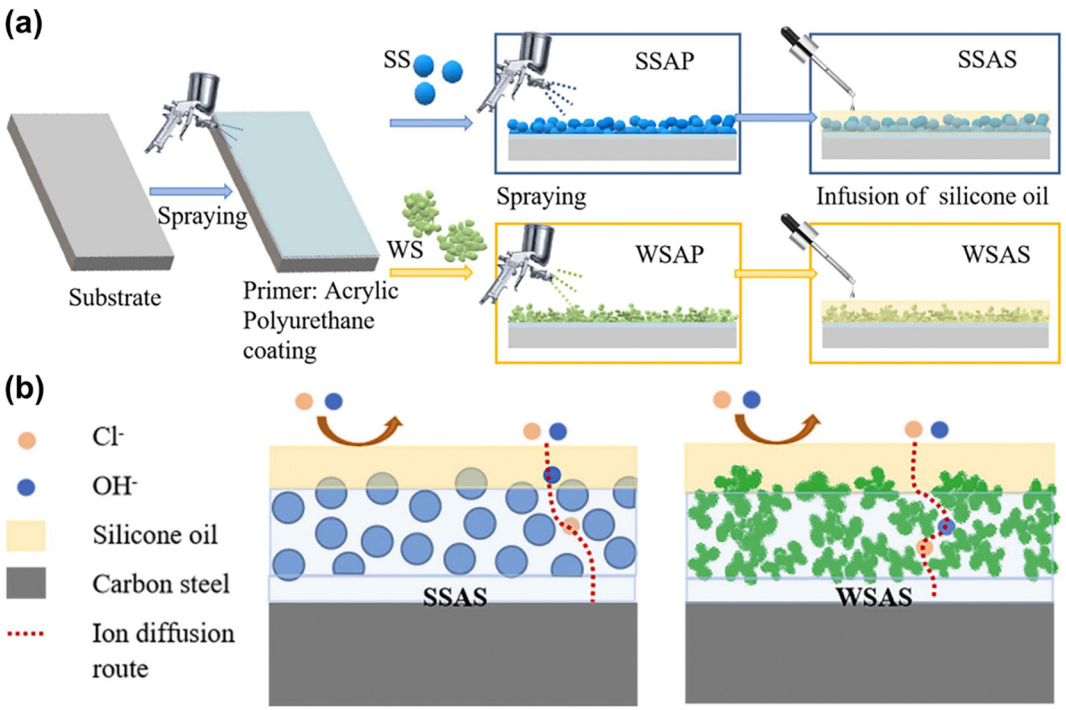

Fig. 16 (a) The schematic image of the preparation process, and (b) schematic protection mechanism of coatings on carbon steel (reproduced from ref. 194 with permission from [Elsevier], copyright [2023]).

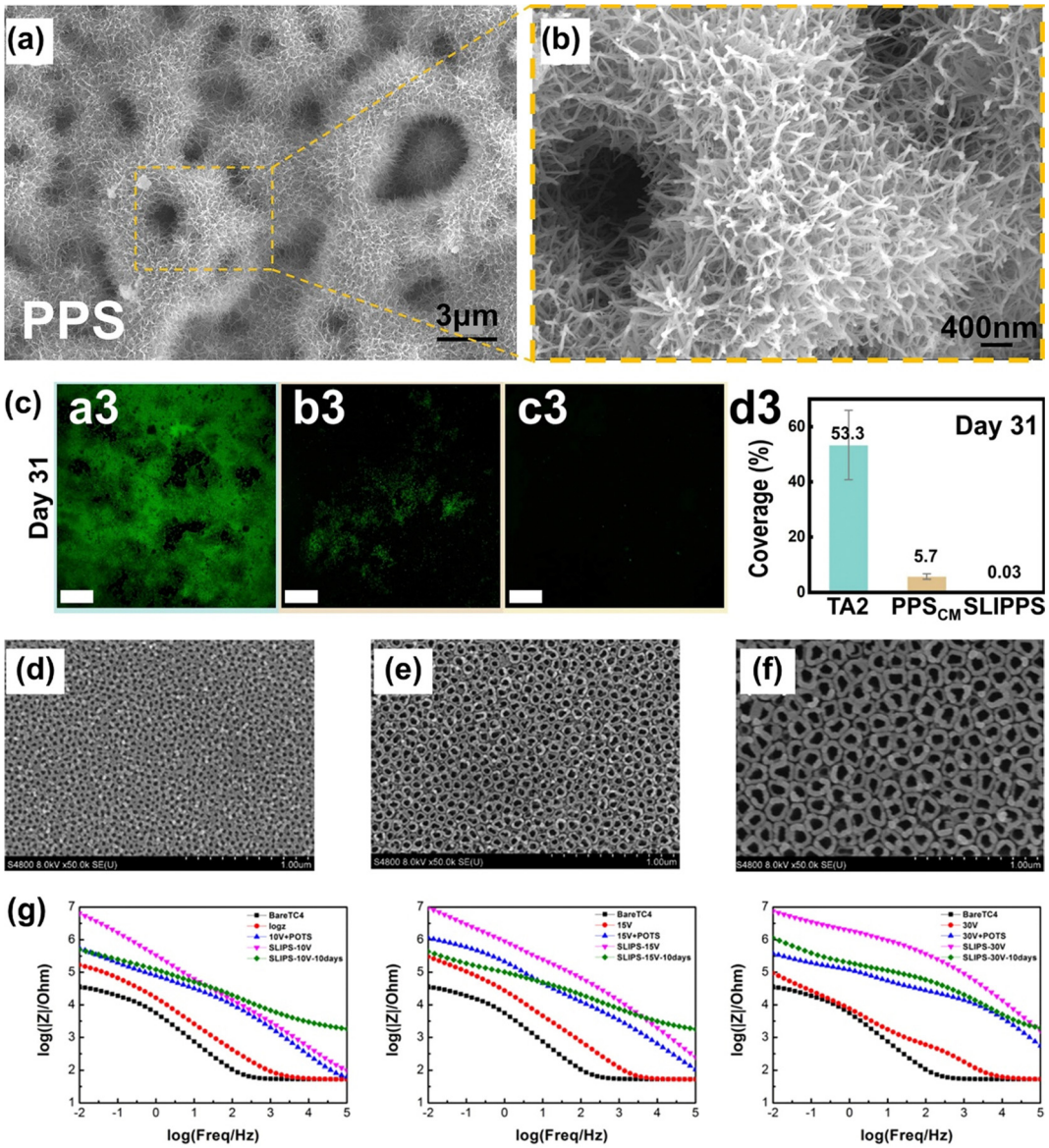

Fig. 17 (a) and (b) SEM images of the surface morphologies of the PPS. (c) CLSM images of the Chlorella covering (reproduced from ref. 198 with permission from [Elsevier], copyright [2023]). (d)–(f) FE-SEM images of the TC4 anodic films formed at different voltages (10 V, 15 V, and 30 V). (g) Electrochemical impedance spectra of samples immersed in 3.5 wt% NaCl solution for 10 days (reproduced from ref. 199 with permission from [American Chemical Society], copyright [2019]).

−850 mV to −500 mV, signifying a substantial improvement in corrosion resistance. Additionally, the impedance value of the super-slippery surface remained two orders of magnitude larger than that of copper foil even after prolonged seawater exposure, validating the long-term protective capability of the super-slippery surface. Wang *et al.*[203] employed the immersion method to directly grow a graphdiyne layer on a copper substrate, as a protective layer in artificial seawater with a corrosion inhibition rate of ~99.75%. To further enhance the coating's protective properties, the Graphdiyne layer was fluorinated, forming SLIPSs with a remarkable corrosion inhibition rate of 99.99%. Hussain *et al.*[188] electrodeposited a layer of Ni–TiO_2 micro-nano rough structure on the copper sheet's surface, modified it with fatty acids, and injected the Krytox lubricant to create a smooth, lubricant-injected surface. This surface exhibited excellent long-term corrosion resistance, with SLIPSs demonstrating a higher corrosion resistance (4.1×10^6 Ω cm^{-2}) compared to the fatty acid-modified Ni–TiO_2 surface (1.9×10^5 Ω cm^{-2}). Ryu *et al.*[204] initially prepared nano-rod-like $Cu(OH)_2$ *via* alkaline chemical etching to establish a microstructure and conditions for lubricant storage (Fig. 18). Introducing silica nanoparticles using the LBL method effectively prevented acidic substances from contacting the underlying nano-structures, addressing surface acid resistance issues. Compared with the unmodified copper tube's heat transfer performance, the SLIPSs on the copper substrate exhibited a higher heat transfer coefficient and was resistant to dust pollution due to its excellent self-cleaning performance.

4.3.4. Aluminum alloys. Aluminum alloys are widely utilized for their lightweight, high strength, good thermal and electrical conductivity, and corrosion resistance.[205] With a density of approximately one-third that of steel, aluminum alloys offer crucial advantages in applications requiring weight reduction, making them ideal for fuel consumption reduction and achieving increased load capacity in aerospace and automotive industries. Aluminum alloys can form a stable oxide film in the air, exhibiting good corrosion resistance. Moreover, when damaged, the oxide film automatically repairs itself, extending the service life of the aluminum alloy.[206,207] However, aluminum alloys are susceptible to corrosion in certain environments, such as acids, alkalis, and seawater, necessitating appropriate protective measures under these specific conditions. The anodizing process of aluminum alloys has a well-established preparation process and can be scaled up to meet commercial standards. The external porous layer ensures a stable lubricant-locking capability. Chen *et al.*[180] introduced a layer of a polyionogel membrane, maintaining capillary force on the pore wall of the anodized aluminum layer. Stable bonding between the aluminum anodized porous surface and the polyionogel membrane was achieved through alkene polymerization with a coupling agent containing vinyl silane and an ionic liquid. Simultaneously, a strong intermolecular interaction formed between the unpolymerized ionic liquid and the polyionogel membrane. Through capillary action and intermolecular interactions, the unpolymerized ionic liquid is locked on the porous surface of the anodized aluminum, serving as the lubricating layer of the sliding sleeve, which effectively inhibits corrosion from the external environment. Sakuraba *et al.*[208] initially prepared a nano-porous anodic alumina layer through an anodic oxidation method and then expanded the pore size by soaking it in a phosphoric acid solution (Fig. 19). After low surface energy treatment, the layer was infused with a lubricant containing organic additives that adsorbed on the porous surface, resulting in self-lubricating SLIPSs. Even in a corrosion system of acetic acid and sodium chloride mixed solution, the organic molecules added, if there are scratch defects on the surface, can be adsorbed again, maintaining high corrosion resistance and self-healing ability. Besides anodizing, SLIPSs can also be constructed using electrodeposition, chemical etching, and LDH methods to enhance the corrosion protection performance of aluminum due to its active characteristics.

4.3.5. Magnesium alloys. Magnesium alloys are widely utilized in engineering applications due to their low elastic modulus, high specific strength, and vibration reduction capabilities.[209] With advancements in low-cost production technology and efficient processing methods for magnesium alloys, coupled with the increasing demand for lightweight and energy-saving materials, magnesium alloys have garnered

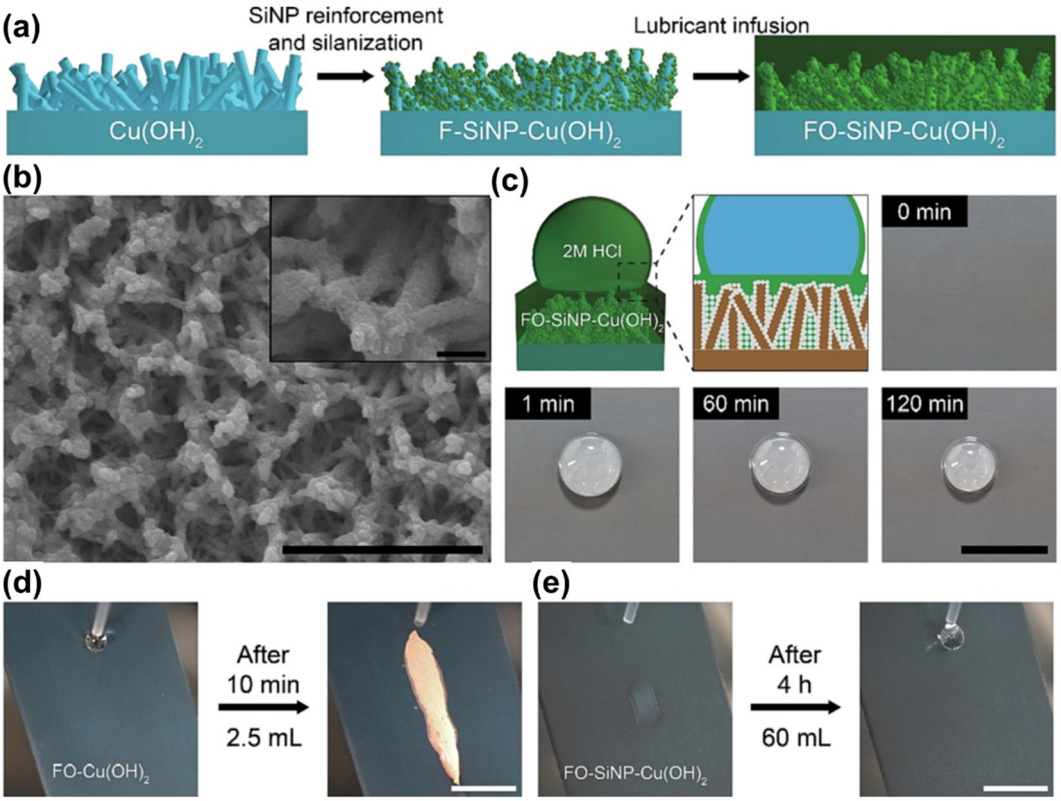

Fig. 18 (a) Schematic illustrating the fabrication process of the SiNP-reinforced SLIPSs. (b) Low and high magnification electron micrographs of SiNP-reinforced SLIPSs. (c) Schematic and series of photographs showing the enhanced acid stability of SiNP-reinforced SLIPSs upon deposition of 2 M HCl droplet (100 μL). The scale bar represents 10 mm. (d) and (e) Acid resistance evaluation *via* continuous dispensing of 2 M HCl droplets on (d) SLIPSs and (e) SiNP-reinforced SLIPSs mounted at a tilting angle of 45° (reproduced from ref. 204 with permission from [Elsevier], copyright [2022]).

significant attention in industries such as aviation, aerospace, and 3C.[210] Similar to aluminum alloys, magnesium alloys naturally form thin oxide films when exposed to air. However, the oxide films on the surface of magnesium alloys are not dense enough to effectively protect the magnesium alloy matrix.[211] Consequently, magnesium alloys are susceptible to galvanic corrosion, environmental corrosion, and other forms of corrosion, limiting their widespread use. Enhancing the corrosion resistance of magnesium alloys has thus become a crucial challenge for their extensive application. One effective approach to improving corrosion resistance is the implementation of SLIPSs on the surface of magnesium and its alloys.

Yao *et al.*[212] performed the *in situ* synthesis of MgAl-LDH nanovessels on the AZ31 magnesium alloy using the hydrothermal method. Sodium benzoate was intercalated into MgAl-LDH as an environmentally friendly corrosion inhibitor. The MgAl-LDH coating was then chemically modified to be superhydrophobic, and SiO_2 nanoparticles, along with silicone oil, were mixed and injected into the superhydrophobic coating to form a composite SiO_2-SLIPS eventually. The surface displayed good corrosion resistance (2.43×10^{-10} A cm^{-2}) and wear resistance (0.041 mm^3). Telmenbayar *et al.*[177] created a layer of a PEO film on the surface of the magnesium alloy using the plasma electrolytic oxidation method. The Zn-MOF film was *in situ* grown on the surface of PEO (Fig. 20(a)–(e)). PEO-MOF-SLIPSs were obtained after modification and injection of a lubricant. After soaking for 7 days, the coating exhibited good corrosion resistance. Furthermore, the prepared coating demonstrated excellent robustness and stability, remaining hydrophobic even after undergoing 100 cm at a 100 g load and 80 cm at a 200 g load on 800 grid sandpaper. Joo *et al.*[213] prepared a nano-porous hydroxide surface structure on the magnesium alloy substrate through plasma electrolytic oxidation and the hydrothermal method. They then constructed a super-slippery surface after modification and lubricating oil infiltration. The results demonstrated that in a 3.5 wt% NaCl solution, SLIPSs significantly enhanced the corrosion resistance of the magnesium alloy, with its corrosion current density being 5 orders of magnitude lower than that of the magnesium alloy matrix.

5. Summary and outlook

Significant progress has been achieved in the research and development of biomimetic self-healing coatings for corrosion prevention applications. However, opportunities for further development exist, especially in repairing large-scale or more complex damage defects. Strategies to improve the transport path of the coating matrix during corrosion or increase the active agent loading can be employed to develop self-healing solutions applicable to larger defects while maintaining overall barrier properties. Future research should focus on bionic self-healing coatings that are more sensitive to external and internal environmental stimuli, allowing quicker responses to maximize repair time and efficiency. Limited research exists on the corrosion resistance and anti-fatigue behavior of intrinsically self-healing materials, necessitating further exploration in this area. An unaddressed issue is the increase in the volume of self-healing coatings when the active agent is released, potentially

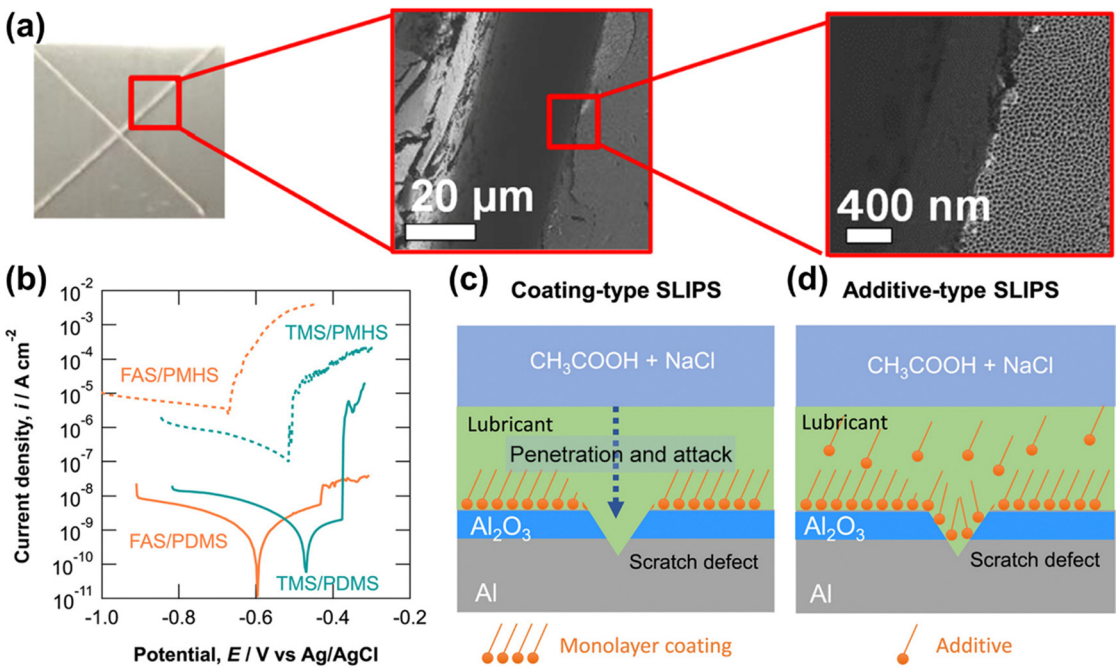

Fig. 19 Potentiodynamic polarization curves of the additive-type SLIPSs measured after immersion in 2 g dm^{-3} acetic acid containing 10 g dm^{-3} NaCl (pH 3) for one week and subsequent introduction of the scratch defects, and schematic illustrations of coating-type and additive-type SLIPSs with a scratch defect (reproduced from ref. 208 with permission from [American Chemical Society], copyright [2021]).

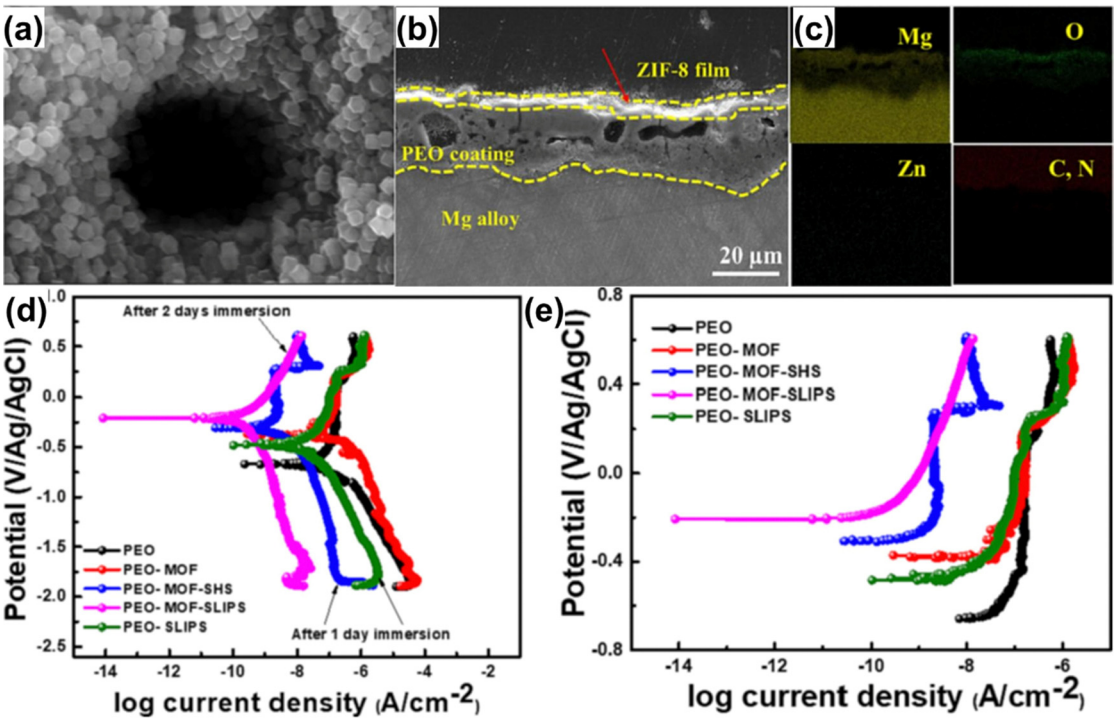

Fig. 20 (a) and (f) Cross-sectional SEM images and elemental mapping analysis of the PEO-MOF sample. (g) and (h) Potentiodynamic polarization curves of different coatings in 3.5 wt% NaCl solution (reproduced from ref. 177 with permission from [Elsevier], copyright [2023]).

creating a diffusion path for corrosive substances and leading to further coating failure and exploring methods to enable automatic coating shrinkage after the release of the active agent is an intriguing area of research.

Reviewing recent research on SHSs and SLIPSs reveals that despite various types applying to different metal substrates, many existing techniques face challenges like high costs, complex processes, limited generalization, and difficulties in scaling up production. The durability of these surfaces remains a significant hurdle, restricting practical applications. While some progress has been made in enhancing durability, it falls short of meeting engineering requirements. The development of both SHSs and SLIPSs has reached a bottleneck, primarily due to limited research being confined to laboratory-scale applications. Future research should prioritize environmentally friendly and cost-effective materials, rational preparation routes, and optimized methods for large-scale, low-cost, and easy preparation. Additionally, exploring new approaches to enhance mechanical stability and long-term durability, particularly for materials capable of self-repairing surface damage caused by friction and wear, will be a prominent area of future research.

Current research on the corrosion resistance or other functions of SHSs or SLIPSs has predominantly focused on replicating outermost surface functions found in organisms, such as hydrophobic effects and oily films. However, organism structures are complex, with a synergistic relationship between functions and structures. For example, fish has specialized epithelial cells secreting mucus for lubrication and defense against adhesive invasion. The outer surface of scaly fish skin, like carp, includes an ultrathin mineral layer on mineralized collagen fibrils, enhancing damage tolerance and serving as exceptional dermal armor.[214] Adopting a multidimensional approach to designing bionic surface structures that integrate both structure and function can provide further inspiration for innovative surfaces.

Conflicts of interest

There are no conflicts to declare.

Acknowledgements

This work is supported by the National Science Foundation of China under the Grant no. 12127806, 62175195, and the International Joint Research Laboratory for Micro/Nano Manufacturing and Measurement Technologies.

References

1 P. Rajala, D. Q. Cheng, S. A. Rice and F. M. Lauro, *Microbiome*, 2022, **10**, 4.
2 L. Yan, Y. Diao, Z. Lang and K. Gao, *Sci. Technol. Adv. Mater.*, 2020, **21**, 359–370.
3 C. Cardell and I. Guerra, *Sci. Adv.*, 2022, **8**, eabn2541.
4 D. Zhang, Y. Liu, R. Liu, X. Guan, S. Xing, X. Dou, Z. He and X. Zhang, *Front. Chem.*, 2022, **10**, 950768.
5 H. Li, W. Song, X. Cui, Y. Li, B. Hou, L. Cheng and P. Zhang, *Nanoscale Res. Lett.*, 2021, **16**, 10.

6 L. Zeng, Y. Chang, Y. Wu, J. Yang, J. F. Xu and X. Zhang, *Sci. Adv.*, 2020, **6**, eaba7524.
7 S. Hong, Z. Wei, K. Wang, W. Gao, Y. Wu and J. Lin, *Ultrason. Sonochem.*, 2021, **72**, 105438.
8 A. Vigneron, E. B. Alsop, B. Chambers, B. P. Lomans, I. M. Head and N. Tsesmetzis, *Appl. Environ. Microbiol.*, 2016, **82**, 2545–2554.
9 C. Liu, B. Qian, P. Hou and Z. Song, *ACS Appl. Mater. Interfaces*, 2021, **13**, 4429–4441.
10 A. López-Ortega, O. Areitioaurtena, S. A. Alves, A. M. Goitandia, I. Elexpe, J. L. Arana and R. Bayón, *Prog. Org. Coat.*, 2019, **137**, 105376.
11 A. S. Jagadeeswar, S. Kumar, B. Venkataraman, P. S. Babu and A. Jyothirmayi, *Surf. Coat. Technol.*, 2020, **399**, 126138.
12 G. Stremsdoerfer, H. Omidvar, P. Roux, Y. Meas and R. Ortega-Borges, *J. Alloys Compd.*, 2008, **466**, 391–397.
13 M. Kultamaa, K. Mönkkönen, J. J. Saarinen and M. Suvanto, *Coatings*, 2021, **11**, 949.
14 H. Eivaz Mohammadloo, A. A. Sarabi, H. R. Asemani and P. Ahmadi, *Prog. Org. Coat.*, 2018, **125**, 432–442.
15 K. Dong, Y. Song, D. Shan and E.-H. Han, *Mater. Corros.*, 2018, **69**, 481–491.
16 D. Zhao, J. Sun, L. Zhang, Y. Tan and J. Li, *J. Rare Earths*, 2010, **28**, 371–374.
17 S. Yu, L. Wang, C. Wu, T. Feng, Y. Cheng, Z. Bu and S. Zhu, *J. Alloys Compd.*, 2020, **817**, 153257.
18 Y. Zhang, Y. Chen, X. Y. Duan, W. Q. Zheng and Y. W. Zhao, *Mater. Res. Express*, 2019, **6**, 126416.
19 M. Cui, B. Wang and Z. Wang, *Adv. Eng. Mater.*, 2019, **21**, 1801379.
20 P. P. Vijayan and D. Puglia, *Emergent Mater.*, 2019, **2**, 391–415.
21 J. S. George, P. Vijayan P, A. T. Hoang, N. Kalarikkal, P. Nguyen-Tri and S. Thomas, *Prog. Org. Coat.*, 2022, **168**, 106858.
22 P. Nguyen-Tri, H. N. Tran, C. O. Plamondon, L. Tuduri, D.-V. N. Vo, S. Nanda, A. Mishra, H.-P. Chao and A. K. Bajpai, *Prog. Org. Coat.*, 2019, **132**, 235–256.
23 Z. Wang, L. Scheres, H. Xia and H. Zuilhof, *Adv. Funct. Mater.*, 2020, **30**, 1908098.
24 J. S. George, P. Vijayan P, J. K. Paduvilan, N. Salim, J. Sunarso, N. Kalarikkal, N. Hameed and S. Thomas, *Prog. Org. Coat.*, 2022, **162**, 106571.
25 I. Martin-Martin, A. Paige, P. C. Valenzuela Leon, A. G. Gittis, O. Kern, B. Bonilla, A. C. Chagas, S. Ganesan, L. B. Smith, D. N. Garboczi and E. Calvo, *Nat. Commun.*, 2020, **11**, 2911.
26 A. Stanley, E. D. Tichy, J. Kocan, D. W. Roberts, E. M. Shore and F. Mourkioti, *NPJ Regener. Med.*, 2022, **7**, 5.
27 E. V. Skorb, D. Fix, D. V. Andreeva, H. Möhwald and D. G. Shchukin, *Adv. Funct. Mater.*, 2009, **19**, 2373–2379.
28 S. R. White, N. R. Sottos, P. H. Geubelle, J. S. Moore, M. R. Kessler, S. R. Sriram, E. N. Brown and S. Viswanathan, *Nature*, 2001, **409**, 794–797.
29 Y.-K. Song, H.-W. Kim and C.-M. Chung, *Polymers*, 2022, **14**, 2013.
30 B. Oktay, J. H. Türkcan, O. K. Özdemir and N. Kayaman-Apohan, *Macromol. Res.*, 2023, **31**, 1077–1086.
31 N. Z. Tomić, A. N. Mustapha, M. AlMheiri, N. AlShehhi and A. Antunes, *Prog. Org. Coat.*, 2022, **172**, 107070.
32 H. Wang, J. Xu, H. Wang, X. Cheng, S. Wang and Z. Du, *Prog. Org. Coat.*, 2022, **167**, 106837.
33 H. Li, Y. Feng, Y. Cui, Y. Ma, Z. Zheng, B. Qian, H. Wang, A. Semenov and D. Shchukin, *Prog. Org. Coat.*, 2020, **145**, 105684.
34 M. Attaei, L. M. Calado, M. G. Taryba, Y. Morozov, R. A. Shakoor, R. Kahraman, A. C. Marques and M. F. Montemor, *Prog. Org. Coat.*, 2020, **139**, 105445.
35 J. Sun, J. Duan, X. Liu, X. Dong, Y. Zhang, C. Liu and B. Hou, *Appl. Mater. Today*, 2022, **28**, 101551.
36 G. Chen, Z. Sun, Y. Wang, J. Zheng, S. Wen, J. Zhang, L. Wang, J. Hou, C. Lin and Z. Yue, *Prog. Org. Coat.*, 2020, **140**, 105483.
37 J. Sun, C. Liu, J. Duan, J. Liu, X. Dong, Y. Zhang, N. Wang, J. Wang and B. Hou, *J. Mater. Sci. Technol.*, 2022, **124**, 1–13.
38 W. Wang, L. Xu, X. Li, Y. Yang and E. An, *Corros. Sci.*, 2014, **80**, 528–535.
39 W. Wang, W. Li, L. Song, W. Fan, C. Xiong, X. Gao, X. Zhang and X. Liu, *J. Electrochem. Soc.*, 2017, **164**, C635.
40 Y. Feng, Y. Cui, M. Zhang, M. Li and H. Li, *Macromol. Mater. Eng.*, 2021, **306**, 2000581.
41 A. R. Hamilton, N. R. Sottos and S. R. White, *Adv. Mater.*, 2010, **22**, 5159–5163.
42 A. Adli, K. Shelesh-Nezhad, M. Khoshravan Azar and M. Mohammadi-Aghdam, *Plast., Rubber Compos.*, 2020, **49**, 79–90.
43 S. J. Pety, J. E. Aw, A. C. Gendusa, P. R. Barnett, Q. A. Calvert, N. R. Sottos and S. R. White, *Compos. Struct.*, 2018, **184**, 428–436.
44 V. Vahedi, P. Pasbakhsh, C. S. Piao and C. E. Seng, *J. Mater. Chem. A*, 2015, **3**, 16005–16012.
45 G. Postiglione, M. Alberini, S. Leigh, M. Levi and S. Turri, *ACS Appl. Mater. Interfaces*, 2017, **9**, 14371–14378.
46 C. J. Hansen, W. Wu, K. S. Toohey, N. R. Sottos, S. R. White and J. A. Lewis, *Adv. Mater.*, 2009, **21**, 4143–4147.
47 C. J. Hansen, S. R. White, N. R. Sottos and J. A. Lewis, *Adv. Funct. Mater.*, 2011, **21**, 4320–4326.
48 J. F. Patrick, M. J. Robb, N. R. Sottos, J. S. Moore and S. R. White, *Nature*, 2016, **540**, 363–370.
49 R. C. R. Gergely, W. A. Santa Cruz, B. P. Krull, E. L. Pruitt, J. Wang, N. R. Sottos and S. R. White, *Adv. Funct. Mater.*, 2018, **28**, 1704197.
50 H. Pulikkalparambil, S. Siengchin and J. Parameswaranpillai, *Nano-Struct. Nano-Objects*, 2018, **16**, 381–395.
51 S. Sinha-Ray, D. D. Pelot, Z. P. Zhou, A. Rahman, X. F. Wu and A. L. Yarin, *J. Mater. Chem.*, 2012, **22**, 9138–9146.
52 H. Wang, H. Cai, B. Chen and C. Mao, *Polym. Compos.*, 2021, **42**, 3281–3292.
53 C. Mao, H. Cai, Y. Gan and M. Li, *Polym. Compos.*, 2023, **44**, 3435–3451.
54 M. W. Lee, S. S. Yoon and A. L. Yarin, *ACS Appl. Mater. Interfaces*, 2016, **8**, 4955–4962.

55 Y. Zhang, J. Ye, D. Qu, H. Wang, C. Chai and L. Feng, *Polym. Eng. Sci.*, 2021, **61**, 2257–2266.
56 M. Uzaki and M. Shibata, *J. Polym. Res.*, 2022, **29**, 453.
57 M. Vauthier, L. Jierry, J. C. Oliveira, L. Hassouna, V. Roucoules and F. Bally-Le Gall, *Adv. Funct. Mater.*, 2019, **29**, 1806765.
58 N. Patra, N. Mameda and M. Salerno, in *Polymer-Based Nanoscale Materials for Surface Coatings*, ed. S. Thomas and J. S. George, Elsevier, 2023, pp. 59–73.
59 P. Poornima Vijayan, J. S. George and R. V. Revathy, in *Multifunctional Epoxy Resins: Self-Healing, Thermally and Electrically Conductive Resins*, ed. N. Hameed, J. C. Capricho, N. Salim and S. Thomas, Springer Nature Singapore, Singapore, 2023, pp. 161–174.
60 S.-L. Xiang, Q.-X. Hua, P.-J. Zhao, W.-L. Gong, C. Li and M.-Q. Zhu, *Chem. Mater.*, 2019, **31**, 5081–5088.
61 M. A. North, C. A. Del Grosso and J. J. Wilker, *ACS Appl. Mater. Interfaces*, 2017, **9**, 7866–7872.
62 B. Qian, Z. Zheng, M. Michailids, N. Fleck, M. Bilton, Y. Song, G. Li and D. Shchukin, *ACS Appl. Mater. Interfaces*, 2019, **11**, 10283–10291.
63 H. Zhang, W. Sun, L. Wang, S. Ma, W. Xing, K. Liang and G. Liu, *Chem. Eng. J.*, 2023, **473**, 145164.
64 W. Chen, J. Fan, Y. Jiang, S. Li, Y. Ying and H. Yang, *Front. Mater.*, 2022, **9**, 850362.
65 H. D. Zhang, A. Y. Chen, B. Gan, H. Jiang and L. J. Gu, *J. Magnesium Alloys*, 2022, **10**, 1358–1367.
66 J. Li, S. Li, C. Chen, H. Guo, B. Lei, P. Zhang, G. Meng and Z. Feng, *Colloids Surf., A*, 2023, **666**, 131283.
67 J. Huang, W. Zhang, H. Li, X. Yu, S. Ding and C. Wu, *J. Mater. Sci.*, 2020, **55**, 17255–17265.
68 L. Song, Z. Gao, Q. Sun, G. Chu, H. Shi, N. Xu, Z. Li, N. Hao, X. Zhang, F. Ma and L. Wang, *Prog. Org. Coat.*, 2023, **175**, 107331.
69 L. Ma, J. Wang, D. Zhang, Y. Huang, L. Huang, P. Wang, H. Qian, X. Li, H. A. Terryn and J. M. C. Mol, *Chem. Eng. J.*, 2021, **404**, 127118.
70 Z. Chen, W. Yang, X. Yin, Y. Chen, Y. Liu and B. Xu, *Prog. Org. Coat.*, 2020, **146**, 105750.
71 S. Habib, A. Hassanein, R. Kahraman, E. Mahdi Ahmed and R. A. Shakoor, *Mater. Des.*, 2021, **207**, 109839.
72 H. H. Zhang, X. Zhang, H. Bian, L. Zhang, Y. Chen, Y. Yang and Z. Zhang, *Colloids Surf., A*, 2024, **682**, 132844.
73 S. Habib, E. Fayyad, M. Nawaz, A. Khan, R. A. Shakoor, R. Kahraman and A. Abdullah, *Nanomaterials*, 2020, **10**, 791.
74 S. Habib, E. Fayyed, R. A. Shakoor, R. Kahraman and A. Abdullah, *Arabian J. Chem.*, 2021, **14**, 102926.
75 A. Khan, A. Hassanein, S. Habib, M. Nawaz, R. A. Shakoor and R. Kahraman, *ACS Appl. Mater. Interfaces*, 2020, **12**, 37571–37584.
76 D. Li, J. Zhuang, Z. Lin, D. Song, Q. Liu, J. Zhu, J. Yu, J. Liu, R. Chen and J. Wang, *Prog. Org. Coat.*, 2023, **185**, 107944.
77 L. Cheng, C. Liu, H. Wu, H. Zhao and L. Wang, *J. Colloid Interface Sci.*, 2022, **606**, 1572–1585.
78 P. Najmi, N. Keshmiri, M. Ramezanzadeh and B. Ramezanzadeh, *Chem. Eng. J.*, 2021, **412**, 128637.
79 A. Dehghani, G. Bahlakeh, B. Ramezanzadeh and A. H. J. Mofidabadi, *J. Environ. Chem. Eng.*, 2021, **9**, 105457.
80 M. Akbari, R. Naderi and B. Ramezanzadeh, *Appl. Mater. Today*, 2023, **33**, 101880.
81 L. Cao, W. Wang, J. Cheng, T. Wang, Y. Zhang, L. Wang, W. Li and S. Chen, *ACS Appl. Mater. Interfaces*, 2023, **15**, 48645–48659.
82 C. Ma, J. Li, J. Wang, D. Bian and Y. Zhao, *Polym. Eng. Sci.*, 2022, **62**, 4173–4184.
83 S. Mohammadkhah, M. Ramezanzadeh, H. Eivaz Mohammadloo, B. Ramezanzadeh and R. Ghamsarizade, *J. Ind. Eng. Chem.*, 2023, **121**, 358–377.
84 C. Zhao, Y. Hu and W. Guo, *Colloids Surf., A*, 2023, **675**, 132018.
85 L. Shen, W. Xie, C. Ni, Y. Xie, L. Miao and W. Zhao, *Mater. Today Nano*, 2023, **24**, 100395.
86 Z. Chen, W. Yang, Y. Chen, X. Yin and Y. Liu, *J. Colloid Interface Sci.*, 2020, **579**, 741–753.
87 H. E. Fathabadi, M. Ghorbani and H. M. Ghartavol, *Nano-Struct. Nano-Objects*, 2021, **26**, 100760.
88 X. Li, B. Gong, J. Zhang, Y. Di, Y. Ding, Z. Chen and W. Yang, *Colloids Surf., A*, 2023, **674**, 131899.
89 J. Yong, Q. Yang, X. Hou and F. Chen, *Ultrafast Sci.*, 2022, **2**, 9895418.
90 D. Zhang, F. Chen, Q. Yang, J. Si and X. Hou, *Soft Matter*, 2011, **7**, 8337–8342.
91 J. Yong, S. C. Singh, Z. Zhan, F. Chen and C. Guo, *Langmuir*, 2019, **35**, 921–927.
92 J. Yong, C. Zhang, X. Bai, J. Zhang, Q. Yang, X. Hou and F. Chen, *Adv. Mater. Interfaces*, 2020, **7**, 1901931.
93 T. Liu, Y. Yin, S. Chen, X. Chang and S. Cheng, *Electrochim. Acta*, 2007, **52**, 3709–3713.
94 J. Yong, F. Chen, Y. Fang, J. Huo, Q. Yang, J. Zhang, H. Bian and X. Hou, *ACS Appl. Mater. Interfaces*, 2017, **9**, 39863–39871.
95 L. B. Boinovich, A. M. Emelyanenko, A. D. Modestov, A. G. Domantovsky and K. A. Emelyanenko, *Mendeleev Commun.*, 2017, **27**, 254–256.
96 X. Lai, J. Hu and J. Qu, *Carbon*, 2023, **212**, 118155.
97 D. Wei, J. Wang, S. Li, D. Wang and Y. Liu, *Chem. Eng. J.*, 2023, **475**, 146113.
98 W. Gu, W. Li, Y. Zhang, Y. Xia, Q. Wang, W. Wang, P. Liu, X. Yu, H. He, C. Liang, Y. Ban, C. Mi, S. Yang, W. Liu, M. Cui, X. Deng, Z. Wang and Y. Zhang, *Nat. Commun.*, 2023, **14**, 5953.
99 Q. Zhang, X. Bai, Y. Li, X. Zhang, D. Tian and L. Jiang, *ACS Nano*, 2022, **16**, 16843–16852.
100 X. Yan, B. Ji, L. Feng, X. Wang, D. Yang, K. F. Rabbi, Q. Peng, M. J. Hoque, P. Jin, E. Bello, S. Sett, M. Alleyne, D. M. Cropek and N. Miljkovic, *ACS Nano*, 2022, **16**, 12910–12921.
101 T. Zheng, Y. Hu, F. Pan, Y. Zhang and A. Tang, *J. Magnesium Alloys*, 2019, **7**, 193–202.
102 H. Wang, Y. Zhu, Z. Hu, X. Zhang, S. Wu, R. Wang and Y. Zhu, *Chem. Eng. J.*, 2016, **303**, 37–47.
103 Y. Zou, Y. Wang, S. Xu, T. Jin, D. Wei, J. Ouyang, D. Jia and Y. Zhou, *Chem. Eng. J.*, 2019, **362**, 638–649.

104 B. Zhang, Q. Zhu, Y. Li and B. Hou, *Chem. Eng. J.*, 2018, **352**, 625–633.
105 Z. Bai and J. Zhu, *Coatings*, 2023, **13**, 1151.
106 Y. Wan, M. Chen, W. Liu, X. Shen, Y. Min and Q. Xu, *Electrochim. Acta*, 2018, **270**, 310–318.
107 W. Tong and D. Xiong, *Mater. Today Phys.*, 2022, **23**, 100651.
108 L. B. Boinovich, E. B. Modin, A. R. Sayfutdinova, K. A. Emelyanenko, A. L. Vasiliev and A. M. Emelyanenko, *ACS Nano*, 2017, **11**, 10113–10123.
109 V. A. Luchkina, M. S. Min'kin, A. Y. Luchkin and Y. I. Kuznetsov, *J. Magnesium Alloys*, 2023, **11**, 3272–3286.
110 W. Tong, L. Cui, R. Qiu, C. Yan, Y. Liu, N. Wang and D. Xiong, *J. Mater. Sci. Technol.*, 2021, **89**, 59–67.
111 D. Li, L. Ma, B. Zhang and S. Chen, *Chem. Eng. J.*, 2022, **450**, 138429.
112 A. Gong, Y. Zheng, Z. Yang, X. Guo, Y. Gao and X. Li, *Mater. Today Commun.*, 2021, **26**, 101828.
113 B. Zhang, W. Xu, D. Xia, Y. Huang, X. Zhao and J. Zhang, *Colloids Surf., A*, 2020, **596**, 124750.
114 M. Hegde, J. Mohan, M. Q. Mushtaq Warraich, Y. Kavanagh, B. Duffy and E. F. Tobin, *Wear*, 2023, **524–525**, 204766.
115 A. V. Rao, S. S. Latthe, S. A. Mahadik and C. Kappenstein, *Appl. Surf. Sci.*, 2011, **257**, 5772–5776.
116 D.-W. Li, H.-Y. Wang, Y. Liu, D.-S. Wei and Z.-X. Zhao, *Chem. Eng. J.*, 2019, **367**, 169–179.
117 Y. Shen, K. Li, H. Chen, Z. Wu and Z. Wang, *Chem. Eng. J.*, 2021, **413**, 127455.
118 S. M. A. Mousavi and R. Pitchumani, *Corros. Sci.*, 2021, **186**, 109420.
119 S. Wang, C. Hou, M. Wu, X. Li, W. Wang, N. Mitsuzaki and Z. Chen, *Colloids Surf., A*, 2021, **614**, 126185.
120 M. Salehi, M. Mozammel and S. M. Emarati, *Colloids Surf., A*, 2019, **573**, 196–204.
121 H. Yin, H. Liu, X. Guo, Z. Cui, J. Tang, X. Lin and C. Hu, *Vacuum*, 2022, **195**, 110699.
122 Z. Kang, Y. He, J. Sang, H. Hirahara and D. Chen, *Adv. Mater. Interfaces*, 2021, **8**, 2100651.
123 H. Jie, Q. Xu, L. Wei and Y. Min, *Corros. Sci.*, 2016, **102**, 251–258.
124 J. Yong, F. Chen, Q. Yang and X. Hou, *Soft Matter*, 2015, **11**, 8897–8906.
125 R. A. Rajan, S. Rao Konda, C. Sajed Saraj, Y. Hang Lai, G. Verma, Z. Yu, W. Yu, D. Yan and J. Yang, *Appl. Surf. Sci.*, 2022, **573**, 151612.
126 I. Vilaró, J. L. Yagüe and S. Borrós, *ACS Appl. Mater. Interfaces*, 2017, **9**, 1057–1065.
127 C.-H. Chang, M.-H. Hsu, C.-J. Weng, W.-I. Hung, T.-L. Chuang, K.-C. Chang, C.-W. Peng, Y.-C. Yen and J.-M. Yeh, *J. Mater. Chem. A*, 2013, **1**, 13869–13877.
128 K.-C. Chang, M.-H. Hsu, H.-I. Lu, M.-C. Lai, P.-J. Liu, C.-H. Hsu, W. F. Ji, T. L. Chuang, Y. Wei, J. M. Yeh and W.-R. Liu, *Carbon*, 2014, **66**, 144–153.
129 S. Zachariah, T.-W. Chuo and Y.-L. Liu, *Polymer*, 2018, **155**, 168–176.
130 A. Vicente, P. J. Rivero, U. Urdiroz, P. García, J. Mora, J. F. Palacio, F. J. Palomares and R. Rodríguez, *Polymers*, 2022, **14**, 4356.
131 H. Li, S. Yu and X. Han, *Chem. Eng. J.*, 2016, **283**, 1443–1454.
132 Y. Shu, X. Lu, W. Lu, W. Su, Y. Wu, H. Wei, D. Xu, J. Liang and Y. Xie, *Surf. Coat. Technol.*, 2023, **455**, 129216.
133 S. Jiang, W. Li, J. Liu, J. Jiang, Z. Zhang, W. Shang, N. Peng and Y. Wen, *J. Magnesium Alloys*, 2023, **11**, 3287–3301.
134 H. Jin, L. Tian, W. Bing, J. Zhao and L. Ren, *Prog. Mater. Sci.*, 2022, **124**, 100889.
135 T. P. Manoj, T. P. Rasitha, S. C. Vanithakumari, B. Anandkumar, R. P. George and J. Philip, *Appl. Surf. Sci.*, 2020, **512**, 145636.
136 T. P. Rasitha, S. C. Vanithakumari, D. Nanda Gopala Krishna, R. P. George, R. Srinivasan and J. Philip, *Prog. Org. Coat.*, 2022, **162**, 106560.
137 M. S. Selim, N. A. Fatthallah, M. A. Shenashen, S. A. Higazy, H. R. Madian, M. M. Selim and S. A. El-Safty, *Langmuir*, 2023, **39**, 2333–2346.
138 L. Zhao, R. Chen, J. Liu, Q. Liu, J. Yu, J. Zhu, P. Liu and J. Wang, *Prog. Org. Coat.*, 2023, **183**, 107812.
139 D. Wang, Q. Sun, M. J. Hokkanen, C. Zhang, F.-Y. Lin, Q. Liu, S.-P. Zhu, T. Zhou, Q. Chang, B. He, Q. Zhou, L. Chen, Z. Wang, R. H. A. Ras and X. Deng, *Nature*, 2020, **582**, 55–59.
140 H. Chen, F. Wang, H. Fan, R. Hong and W. Li, *Chem. Eng. J.*, 2021, **408**, 127343.
141 B. Zhang, J. Duan, Y. Huang and B. Hou, *J. Mater. Sci. Technol.*, 2021, **71**, 1–11.
142 J. Zhang, X. Pei, J. Huang, X. Ke, C. Xu, W. Zhao, L. Li, Y. Weng and J. Chen, *ACS Appl. Mater. Interfaces*, 2023, **15**, 265–280.
143 J. F. Ou, X. Z. Fang, W. J. Zhao, S. Lei, M. S. Xue, F. J. Wang, C. Q. Li, Y. L. Lu and W. Li, *Langmuir*, 2018, **34**, 5807–5812.
144 R. Poetes, K. Holtzmann, K. Franze and U. Steiner, *Phys. Rev. Lett.*, 2010, **105**, 166104.
145 A. Manoj, R. Ramachandran and P. L. Menezes, *Int. J. Adv. Manuf. Technol.*, 2020, **110**, 457–470.
146 S. F. Ahmadi, V. Umashankar, Z. Dean, B. Chang, S. Jung and J. B. Boreyko, *ACS Appl. Mater. Interfaces*, 2021, **13**, 27567–27574.
147 L. Zhang, X. Xue, H. Zhang, Z. Huang and Z. Zhang, *Composites, Part A*, 2021, **146**, 106405.
148 H. Teisala, F. Geyer, J. Haapanen, P. Juuti, J. M. Mäkelä, D. Vollmer and H.-J. Butt, *Adv. Mater.*, 2018, **30**, 1706529.
149 Y. Tan, J. Yang, Y. Li, X. Li, Q. Wu, Y. Fan, F. Yu, J. Cui, L. Chen, D. Wang and X. Deng, *Adv. Mater.*, 2022, **34**, 2202167.
150 K. Zhang, F. Xu and Y. Gao, *Appl. Mater. Today*, 2021, **22**, 100970.
151 Y. Liu, Y. Zheng, T. Li, D. Wang and F. Zhou, *Nano Energy*, 2019, **61**, 454–461.
152 X. Han, L. Ren, Y. Ma, X. Gong and H. Wang, *Carbon*, 2022, **197**, 27–39.
153 Y. Wang, Y. Liu, J. Li, L. Chen, S. Huang and X. Tian, *Chem. Eng. J.*, 2020, **390**, 124311.

154 P. C. Uzoma, F. Liu and E.-H. Han, *J. Mater. Sci. Technol.*, 2020, **45**, 70–83.
155 X. Li, B. Li, Y. Li and J. Sun, *Chem. Eng. J.*, 2021, **404**, 126504.
156 X. Ni, Y. Gao, X. Zhang, Y. Lei, G. Sun and B. You, *Chem. Eng. J.*, 2021, **406**, 126725.
157 X. Liu, H. He, T. C. Zhang, L. Ouyang, Y.-X. Zhang and S. Yuan, *Chem. Eng. J.*, 2021, **404**, 127106.
158 Z. Wang, L. Yuan, G. Liang and A. Gu, *Chem. Eng. J.*, 2021, **408**, 127263.
159 X. Bai, Q. Yang, H. Li, J. Huo, J. Liang, X. Hou and F. Chen, *Langmuir*, 2022, **38**, 4645–4656.
160 J. Zhang, X. Zhao, J. Wei, B. Li and J. Zhang, *Langmuir*, 2021, **37**, 13527–13536.
161 J. Zhang, J. Wei, B. Li, X. Zhao and J. Zhang, *J. Colloid Interface Sci.*, 2021, **594**, 836–847.
162 H. F. Bohn and W. Federle, *Proc. Natl. Acad. Sci. U. S. A.*, 2004, **101**, 14138–14143.
163 T.-S. Wong, S. H. Kang, S. K. Y. Tang, E. J. Smythe, B. D. Hatton, A. Grinthal and J. Aizenberg, *Nature*, 2011, **477**, 443–447.
164 Y. Long, X. Yin, P. Mu, Q. Wang, J. Hu and J. Li, *Chem. Eng. J.*, 2020, **401**, 126137.
165 Y. Yu, B. Li, Y. Wei, X. Ren, F. Bie, Y. Xu, R. Qiu, X. Li and Y. Ouyang, *J. Ind. Eng. Chem.*, 2023, **118**, 298–308.
166 Y. Kan, F. Zheng, B. Li, R. Zhang, Y. Wei, Y. Yu, Y. Zhang, Y. Ouyang and R. Qiu, *Colloids Surf., A*, 2021, **630**, 127585.
167 J. Zhang, C. Gu and J. Tu, *ACS Appl. Mater. Interfaces*, 2017, **9**, 11247–11257.
168 P. Wang, T. Li and D. Zhang, *Corros. Sci.*, 2017, **128**, 110–119.
169 J. Wang, Y. Wang, K. Zhang, X. Liu, S. Zhang, D. Wang and L. Xie, *J. Colloid Interface Sci.*, 2024, **659**, 289–298.
170 M. Tonelli, S. Peppou-Chapman, F. Ridi and C. Neto, *J. Phys. Chem. C*, 2019, **123**, 2987–2995.
171 M. J. Hoque, S. Sett, X. Yan, D. Liu, K. F. Rabbi, H. Qiu, M. Qureshi, G. Barac, L. Bolton and N. Miljkovic, *ACS Appl. Mater. Interfaces*, 2022, **14**, 4598–4611.
172 A. Sasidharanpillai, Y. Lee and S. Lee, *Colloids Surf., A*, 2022, **646**, 128923.
173 T. Zhu, Y. Yuan, Q. Yu, H. Xiang, G. Liu, X. Dai and R. Liao, *Mater. Chem. Phys.*, 2023, **306**, 128073.
174 W. Yao, Y. Chen, L. Wu, B. Jiang and F. Pan, *J. Taiwan Inst. Chem. Eng.*, 2022, **131**, 104176.
175 J. Sun, C. Wang, J. Song, L. Huang, Y. Sun, Z. Liu, C. Zhao and Y. Li, *J. Mater. Sci.*, 2018, **53**, 16099–16109.
176 H. Li, X. Fu and X. Chu, *J. Mater. Sci.*, 2022, **57**, 3746–3756.
177 L. Telmenbayar, A. Gopal Ramu, D. Yang and D. Choi, *Chem. Eng. J.*, 2023, **458**, 141397.
178 T. Xiang, M. Zhang, H. R. Sadig, Z. Li, M. Zhang, C. Dong, L. Yang, W. Chan and C. Li, *Chem. Eng. J.*, 2018, **345**, 147–155.
179 Y. Jing, F. Meng, F. Wang and L. Liu, *Appl. Surf. Sci.*, 2023, **639**, 158214.
180 Y. Chen and Z. Guo, *J. Mater. Chem. A*, 2020, **8**, 24075–24085.
181 C. Urata, G. J. Dunderdale, M. W. England and A. Hozumi, *J. Mater. Chem. A*, 2015, **3**, 12626–12630.
182 Y. Liu, W. Sun, K. Feng, Y. Wu, B. Yu, S. Liu and F. Zhou, *Prog. Org. Coat.*, 2023, **174**, 107311.
183 J. Yu, R. Zhao, J. Wang, N. Wang, J. Xu, M. Jin and Y. Zhao, *Tribol. Int.*, 2024, **192**, 109220.
184 H. Zhao, Q. Sun, X. Deng and J. Cui, *Adv. Mater.*, 2018, **30**, 1802141.
185 Y. Liang, C. Li, P. Wang and D. Zhang, *Colloids Surf., A*, 2021, **631**, 127696.
186 T. Zhu, Y. Yuan, Q. Yu, H. Xiang, X. Dai, G. Liu and R. Liao, *J. Ind. Eng. Chem.*, 2023, **127**, 454–466.
187 X. Zhu, J. He, Y. Yao, J. Li, K. Li, X. Liu and M. Qu, *Surf. Coat. Technol.*, 2022, **449**, 128935.
188 M. M. Hussain, A. Kunwar, M. K. Majeed, Y. Wang, A. Saleem and H. Ma, *Adv. Eng. Mater.*, 2021, **23**, 2100266.
189 K. Xing, Z. Li, Z. Wang, S. Qian, J. Feng, C. Gu and J. Tu, *Chem. Eng. J.*, 2021, **418**, 129079.
190 B. Gao, Q. Lai, Y. Cao, R. Hu, L. Xiao, Z. Pan, N. Liang, Y. Li, G. Sha, M. Liu, H. Zhou, X. Wu and Y. Zhu, *Sci. Adv.*, 2020, **6**, eaba8169.
191 T. P. Hoar and W. R. Jacob, *Nature*, 1967, **216**, 1299–1301.
192 T. Xiang, H. Ren, Y. Zhang, Y. Qiang, Y. Yang, C. Li, P. Wang and S. Zhang, *Mater. Des.*, 2022, **215**, 110450.
193 K. Bae, M. Kang, Y. Shin, E. Choi, Y.-M. Kim and J. Lee, *Nanomaterials*, 2023, **13**, 807.
194 K. Zhang, S. Xu, J. Tan, X. Li, L. Du, J. Ma and P. Qiu, *Colloids Surf., A*, 2023, **669**, 131495.
195 S. Yan, G.-L. Song, Z. Li, H. Wang, D. Zheng, F. Cao, M. Horynova, M. S. Dargusch and L. Zhou, *J. Mater. Sci. Technol.*, 2018, **34**, 421–435.
196 W. Q. Zhu, S. Y. Shao, L. N. Xu, W. Q. Chen, X. Y. Yu, K. M. Tang, Z. H. Tang, F. M. Zhang and J. Qiu, *J. Nanobiotechnol.*, 2019, **17**, 55.
197 S. Kumar, F. Ye, B. Mazinani, S. Dobretsov and J. Dutta, *Int. J. Mol. Sci.*, 2021, **22**, 4513.
198 D. Yue, X. Jiang, H. Yu and D. Sun, *Chem. Eng. J.*, 2023, **463**, 142389.
199 Y. Wang, W. Zhao, W. Wu, C. Wang, X. Wu and Q. Xue, *ACS Appl. Bio Mater.*, 2019, **2**, 155–162.
200 T. Yimyai, R. Thiramanas, T. Phakkeeree, S. Iamsaard and D. Crespy, *Adv. Funct. Mater.*, 2021, **31**, 2102568.
201 G. Chilkoor, K. Jawaharraj, B. Vemuri, A. Kutana, M. Tripathi, D. Kota, T. Arif, T. Filleter, A. B. Dalton, B. I. Yakobson, M. Meyyappan, M. M. Rahman, P. M. Ajayan and V. Gadhamshetty, *ACS Nano*, 2020, **14**, 14809–14819.
202 Z. Shi, Y. Ouyang, R. Qiu, S. Hu, Y. Zhang, M. Chen and P. Wang, *Prog. Org. Coat.*, 2019, **131**, 49–59.
203 J. Wang, H. Yan, Y. Zhao, D. Wu, H. Yang, X. Yin, R. Tan and T. Zhang, *ACS Appl. Mater. Interfaces*, 2023, **15**, 12305–12314.
204 M. Ryu, H. Choi, J. Yoon, Y.-N. Choi, S. Lee, H. Kim, M. Chae, J. W. Lee, J. Kang and H. Lee, *Chem. Eng. J.*, 2023, **451**, 138657.
205 C. He, X. Zhao, Y. Lei, J. Nie, X. Lu, J. Song, L. Wang, H. Li, F. Liu, Y. Zhang and Q. Niu, *Mol. Ther.--Nucleic Acids*, 2021, **26**, 1401–1417.
206 Y. Liu, Z. Wang and W. Ke, *Corros. Sci.*, 2014, **80**, 169–176.

207 R. I. Revilla, H. Terryn and I. De Graeve, *Electrochem. Commun.*, 2018, **93**, 162–165.
208 K. Sakuraba, S. Kitano, D. Kowalski, Y. Aoki and H. Habazaki, *ACS Appl. Mater. Interfaces*, 2021, **13**, 45089–45096.
209 B. Y. Liu, Z. Zhang, F. Liu, N. Yang, B. Li, P. Chen, Y. Wang, J. H. Peng, J. Li, E. Ma and Z. W. Shan, *Nat. Commun.*, 2022, **13**, 1060.
210 Y. Yan, X. Liu, H. Xiong, J. Zhou, H. Yu, C. Qin and Z. Wang, *Nanomaterials*, 2020, **10**, 947.
211 S. Leleu, B. Rives, J. Bour, N. Causse and N. Pébère, *Electrochim. Acta*, 2018, **290**, 586–594.
212 W. Yao, J. Qin, Y. Chen, L. Wu, B. Jiang and F. Pan, *Mater. Des.*, 2023, **227**, 111721.
213 J. Joo, D. Kim, H.-S. Moon, K. Kim and J. Lee, *Appl. Surf. Sci.*, 2020, **509**, 145361.
214 H. Quan, W. Yang, M. Lapeyriere, E. Schaible, R. O. Ritchie and M. A. Meyers, *Matter*, 2020, **3**, 842–863.